Repeated degradation and progradation of submarine slope over geological timescales (10^3-10^4 Myr)

Christopher A-L. Jackson[1*]
Andrew E. McAndrew[1§]
David M. Hodgson[2§]
Tom Dreyer[3]

[1]*Basins Research Group (BRG), Department of Earth Science and Engineering, Imperial College, Prince Consort Road, London, SW7 2BP, UK*

[2]*Stratigraphy Group, School of Earth and Environment, University of Leeds, Leeds, LS2 9JT, UK*

[3]*Statoil ASA, Sandsliveien 90, N5020, Bergen, NORWAY*

[§]*present address: ExxonMobil Production*

[*]*corresponding author: c.jackson@imperial.ac.uk (C. Jackson)*

Abstract

Submarine slopes prograde via accretion of sediment to clinoform foresets, and degrade in response to channel or canyon incision, or mass-wasting processes. The timescales over which slope progradation and degradation occur, and the large-scale stratigraphic record of these processes, remain unclear due to a lack of age constraints in subsurface-based studies, and areally limited exposures of exhumed systems. We here integrate 3D seismic reflection and borehole data to study the geometry and origin of ancient slope canyons developed within Late Mesozoic strata of the Måløy Slope, offshore western Norway. Slope degradation and canyon incision commenced during the late Kimmeridgian, coincident with the latter stages of rifting. Subsequent periods of incision and canyon formation (Aptian-to-Albian and Albian-to-Cenomanian) occurring during post-rift subsidence. The canyons are straight, up to 700 m deep and 9 km wide on the upper slope, and die-out downdip onto the lower slope. The canyons trend broadly perpendicular to and crosscut the majority of the rift-related, Late Jurassic normal faults, although syn-incision fault growth locally controlled the depth of basal erosion. The headwalls of the oldest, late Kimmeridgian canyons are located at the fault-controlled shelf edge, whereas the younger Aptian-to-Albian and Albian-to-Cenomanian canyons overstep this fault, which had become inactive by this time, and extend further landward into the immediate hangingwall of a larger, basin-bounding fault system. Further downslope, the younger canyons are superimposed on and truncate older,

underlying canyon-fills. Boreholes indicate that the canyons bases are defined by sharp, erosional surfaces, across which we observe an abrupt upward shift from shallow marine to deep marine facies (i.e. late Kimmeridgian canyons), or deep marine to deep marine facies (Aptian-to-Albian and Albian-to-Cenomanian canyons). Missing biostratigraphic zones indicate the canyons record relatively protracted periods (c. 2-17 Myr) of structurally enhanced slope degradation and sediment bypass, separated by >10 Myr periods of deposition and slope accretion. The trigger for slope degradation is unclear, but likely record basinward tilting of this tectonically active rifted margin, enhanced by incision of the slope by erosive sediment gravity-flows. The results of our study have implications for the timescales over which slope aggradation and degradation occur, and the complex geophysical and geological (i.e. stratigraphic) expression of related features in the rock record. We also demonstrate that canyon formation caused a major reorganisation of rift-related drainage patterns and sediment dispersal, resulting in an abrupt change in syn-rift facies distributions not predicted by existing marine rift-basin tectono-stratigraphic models.

1. Introduction

Submarine slope growth is driven by periods of sediment progradation and aggradation (e.g. Rich, 1951; Bates, 1953; Asquith, 1970; Pirmez et al., 1998; Steckler et al. 1999; Adams and Schlager, 2000; Steel and Olsen, 2002; Patruno et al., 2015; Patruno & Helland-Hansen, 2018). Slope progradation and aggradation may alternate with periods of erosion or 'degradation', during which time erosional conduits, such as channel-levee systems, may bypass large volumes of sediment to the lower slope and basinfloor (e.g. Mayall et al., 2006; Neal & Abreu, 2009; Kane et al., 2009; Romans et al., 2009; Sylvester et al., 2012; Figueiredo et al., 2013; Hodgson et al., 2011, 2016; Janoko et al., 2013; Hubbard et al., 2014). Constraining the location, timing and duration of these degradational periods is important, as they may allow us to infer the driving mechanisms (e.g. tectonics, eustacy), and predict when, where, and how much sediment is transferred downdip (e.g. Johannessen & Steel, 2005; Hodgson et al., 2011; Gong et al., 2015). More generally, establishing whether canyons form in the submarine or subaerial realm is important in terms of assessing basin morphology and paleogeography, and the potential timing and magnitude of tectonic events, and/or changes in eustatic sea-level (e.g. Shepherd, 1981; Posamentier & Vail, 1988; Pratson & Coakley, 1996; Fulthorpe et al., 2000; Bertoni & Cartwright, 2005; Maier et al., 2018). For example, do canyons encased in largely marine strata simply represent subaerially formed 'incised valleys' (*sensu stricto*; Van Wagoner et al., 1998) generated during a period of sea-level fall and lowstand? Or can canyons form at any point in the relative sea-level cycle in a fully submarine setting in response to some kind of tectonic or sediment supply forcing?

Outcrop-based studies permit detailed analysis of the sedimentological and stratigraphic expression of only one or a few cycles of slope aggradation and degradation; however, due to limited exposure the longer-term, larger-scale, three-dimensional geometry of, for example, large (i.e.

kilometre-scale) slope canyons, is poorly constrained (e.g. Wonham et al., 2000; Bertoni & Cartwright, 2005; Giddings et al., 2010; Hodgson et al., 2011, 2016). In contrast, bathymetric maps of the present seabed and near-seabed geophysical studies permit detailed assessment of the geometry and likely formative mechanisms of degradation-related slope conduits, but not their longer-term (10^3-10^4 Myr) stratigraphic development or the processes that controls their ultimate preservation in the rock record. To better constrain the morphology and long-term stratigraphic evolution of submarine canyons, and thus their importance as 'tape records' of allogenic controls (e.g. tectonics, sea-level variations), we require data that permit detailed mapping of age-constrained canyons over large areas.

We here use 3D seismic reflection and borehole data from the North Viking Graben, offshore western Norway to constrain the geometry, distribution, and large-scale stratigraphic evolution of late Mesozoic (Late Jurassic-to-Late Cretaceous) slope canyons through three long-term (i.e. 10^3-10^4 Myr), large-scale (i.e. kilometre-scale) cycles of slope degradation and aggradation (Figs 1 and 2). This is an ideal location to conduct this study, with abundant 3D seismic reflection and borehole data allowing us to map the major structural elements and large-scale stratigraphic patterns, and to thus reconstruct the overall tectono-stratigraphic development of part of this rifted margin. We place our study within a regional, North Sea-wide biostratigraphically constrained, chronostratigraphic framework to investigate the potential regional and local controls on slope canyon formation and evolution. The results of our study have implications for the timescales over which slope aggradation and degradation occur, and the complex geophysical and geological (i.e. stratigraphic) expression of related features in the rock record. Furthermore, our results impact our understanding of rifted margin development, indicating that canyon growth during the syn-rift-post-rift transition drives major changes in drainage patterns and sediment dispersal, resulting in deep-water facies distributions not predicted by existing marine rift-basin tectono-stratigraphic models.

2. Geological Setting of the Måløy Slope

2.1. Structural framework

The Måløy Slope is up to 40 km wide, and is bound to the east by a series of broadly N-trending, W-dipping normal faults that have >1 km of displacement, and which collectively form the Øygarden Fault Complex (Fig. 1). The Måløy Slope is bound on its western margin by a W-dipping normal fault that defines the eastern margin of the Sogn Graben (Figs 3 and 4). A 10-15 km wide graben, herein called the Gjøa Graben, is developed in the middle of the Måløy Slope. The western margin of the Gjøa Graben is delineated by a relatively large (500 ms TWT or 714-973 m of throw), E-dipping, strongly segmented normal fault, herein called the Gjøa Fault (Figs 1 and 3). The eastern margin of the Gjøa Graben is defined by a series of W-dipping, N-trending, moderately large (15 km long, up to 400 m throw) normal faults that together form part of the Måløy Fault System (Figs 3 and 4). Internally, the

Gjøa Graben is dissected by numerous N-S-to-NNW-SSE-striking, E- and W-dipping, relatively small (up to 200 m throw) normal faults (Reeve et al., 2015), whereas several W-dipping, relatively small (up to 360 m throw) normal faults are present into the footwall of the Gjøa Fault (Figs 3 and 4).

2.2. Tectono-stratigraphic framework

The Måløy Slope is underlain by Caledonian metamorphic and igneous rocks, with the oldest sedimentary rocks being Early Jurassic (Statfjord Formation and Dunlin Group; Fig. 2) (e.g. Steel & Ryseth, 1990; Reeve et al., 2015). Middle Jurassic (the Aalenian-to-Bajocian Brent Group) rocks overlie the Early Jurassic sequence (e.g. Sørheim et al., 1990), with the complete succession being up to 300 m thick on the Måløy Slope (Figs 2 and 3) (e.g. Helland-Hansen et al., 1989).

During the early part of the Late Jurassic (Callovian and Oxfordian), flooding of the North Sea Basin resulted in deposition of shallow marine sandstone (Krossfjord, Fensfjord and Sognefjord formations), shelf mudstone and siltstone (Heather Formation), and eventually deep-marine mudstone and sandstone (Draupne Formation) (Fig. 2) (e.g. Helland-Hansen et al., 1989; Dreyer et al., 2005; Patruno et al., 2014; 2015; Holgate et al., 2015). Thickening of the Upper Heather and Draupne formations across many of the normal faults on the Måløy Slope indicates extension and normal faulting likely began during the Kimmeridgian (Fig. 4). Late Jurassic deep-water deposition was interrupted by the formation of a major erosional unconformity, which is herein referred to as the Upper Jurassic Unconformity or UJUNC (Figs. 3 and 4). Although dramatic in terms of its seismic expression, and the impact it had on preservation and thus the ultimate distribution of the underlying Heather and Draupne formations (Fig. 4), the exact geometry and processes responsible for the formation of this and younger unconformities remain unclear (Jackson et al., 2008; Sømme & Jackson, 2013; Sømme et al. 2013; Koch et al., 2017).

During the Early Cretaceous, many of the rift-related normal faults became inactive as the basin underwent a transition from relatively rapid, fault-controlled subsidence to relatively slow, thermal cooling-induced, post-rift subsidence (Gabrielsen et al., 2001; Fraser et al., 2003). In addition, the locus of subsidence migrated westwards into the axis of the Sogn Graben and mainland Norway was uplifted, possibly in response to the initiation of opening of the North Atlantic (Martinsen et al., 1999; Bugge et al., 2001; Gabrielsen et al., 2001). This decline in the rate of normal fault slip and basin subsidence, combined with ongoing deep-water deposition, resulted in healing of underlying rift-related topography. The Måløy Slope thus represented a westward-facing slope during much of the Cretaceous, with the basin floor lying >50 km to the west in the axis of the Sogn Graben (Fig. 1). Although generally considered a period of tectonic quiescence, it is likely the Øygarden Fault Complex was active during the Late Cretaceous (Færseth, 1996; Bell et al., 2014). Furthermore, several authors suggest this major fault controlled the location of the Late Cretaceous shelf-edge (Martinsen et al., 2005; Jackson et al., 2008; Sømme & Jackson, 2013; Sømme et al., 2013). Based on minor offset of Cretaceous seismic

reflection events, it is clear that the Gjøa Fault was also reactivated and accumulated a relatively minor amount of displacement during the Late Cretaceous (Fig. 4A).

The Cretaceous succession on the Måløy Slope is up to 800 m thick and dominated by fine-grained pelagic carbonates and hemipelagic mudstone (Fig. 2) (Bugge et al., 2001; Gabrielsen et al., 2001; Kjennerud et al., 2001; Kyrkjebø et al., 2001). However, during both the Early Cretaceous (Albian) and Late Cretaceous (Late Turonian), a series of sand-rich submarine channels and fans were deposited on the Måløy Slope (Martinsen et al., 1999; Jackson, 2007; Jackson et al., 2008). These depositional systems were fed by material derived from the Norwegian mainland and these sediments were delivered to the slope via a series of shelf-edge canyons, which initially formed during the Late Jurassic (Jackson et al., 2008; Sømme & Jackson, 2013; Sømme et al., 2013).

3. Dataset

We use a 1200 km^2, pre-stack time-migrated, zero-phase processed, 3D seismic reflection dataset to map, in three-dimensions, basin structure and stratigraphy, including the slope canyons and their fill, forming the focus of this study (Figs 1 and 3). A downward increase in acoustic impedance is represented by a peak, and a downward decrease in acoustic impedance is represented by a trough (i.e. SEG normal polarity; Brown, 2011). Inline and crossline spacing are 12.5 m, and the stratigraphic interval of interest lies at 500-3500 milliseconds two-way time (ms TWT); the frequency content of the data at this depth is 25-30 Hz and the average interval velocity is 2600-3175 m/sec, thereby yielding an approximate vertical resolution of *c*. 22-32 m. Seismic data quality varies from good to moderate, and the key rift-related structures and erosional unconformities are relatively well-imaged. Measurements in ms TWT are converted to metres using velocity data taken from wells within the study area. However, marked variations in the depth of burial of the studied succession occur due to the pronounced westward tilt of the basin margin (Fig. 4); we thus use interval velocities of 2600 m/sec and 3175 m/sec to convert values in proximal (i.e. to the east of the Måløy Fault) and distal (i.e. to the west of the Måløy Fault) areas, respectively. A range rather than an absolute value is presented for all measurements to account for ±10% uncertainty in the velocity values used for depth conversion.

We use data from six exploration boreholes to constrain the age, lithology, thickness, and facies of the studied succession (35/9-1, 35/9-2, 35/9-3, 36/7-1, 36/7-2 and 36/7-3; Figs 3-5). These boreholes contain a standard suite of well-log and cuttings data, and one of the boreholes, 36/7-1, has 280 m of core within the interval of interest. In boreholes lacking core data, we use cuttings data to constrain the lithology. Biostratigraphic data, derived principally from micro-palaeontology and palynology, constrain the age of key unconformities identified within the studied succession. These unconformities are related to periods of: (i) *erosion*, being generally defined where stratigraphic units and their associated biostratigraphic events are missing; and (ii) *stratigraphic condensation*, likely caused by marine flooding and/or non-deposition (Fig. 6; see also Table 1).

4. Methods

To delineate the structure of the study area, and the geometry and distribution of the slope canyons associated with late Mesozoic unconformities, we mapped eight seismic horizons within the 3D seismic dataset (Figs 2 and 4). Isochron maps of the key stratal units constrain syn-depositional variations in accommodation, which in this tectonically active basin are principally related to rift-related normal faulting, and to variable preservation of stratigraphic units below and above the late Mesozoic canyons.

Seismic-stratigraphic relationships, in particular reflection truncation and onlap, were used to define the main canyons in seismic data (Fig. 7). Variations in the lithologies overlying and underlying the canyons mean the seismic expression of their basal erosion surface is highly variable in terms of polarity and amplitude. We therefore employed line-by-line seismic mapping to ensure that the geometry of the canyons, and the stratigraphic relationships between individual unconformities, was accurately captured. Seismically-defined unconformities were tied to boreholes using synthetic seismograms. The quality of the seismic-to-borehole ties was considered to be good-to-excellent, with <30 m mismatch between key reflection events expressed on the synthetics, and those identified and mapped in the seismic data (Fig. 8). Several boreholes are located in the footwalls to rift-related in locations where the Upper Jurassic to Lower Cretaceous succession is locally thin or even absent (Figs 3, 4b, 5b-c and 7c). In these locations, the unconformities are not expressed as discrete reflection and the thickness of stratal units they bound fall below the vertical resolution of seismic data. Where this occurs, we assume the major erosional unconformities mapped in the seismic data correlate to the longest duration, biostratigraphically-constrained unconformities identified in boreholes.

5. Subsurface expression of slope canyons

We identify three slope canyon-defining unconformities in the late Mesozoic succession of the Måløy Slope (UC1-3; Figs 2 and 4-7; see also Table 1). In this section, we combine seismic reflection and borehole data to describe the unconformities and related canyons in stratigraphically ascending order. For each unconformity the descriptions are arranged as follows: (i) a description of the stratigraphic (Figs 5 and 6; see also Table 1) and sedimentological (Figs 9 and 10) expression of the canyon-defining unconformity and flanking strata, based on borehole-derived data; (ii) a description of the three-dimensional geometry and geomorphological features associated with the unconformity, based on seismic reflection data (Figs 7 and 13); and (iii) an interpretation of the tectono-stratigraphic setting for the given time period, with an emphasis on the controls on the origin and evolution of the unconformities.

4.1. Unconformity 1 (UC1)

4.1.1. Stratigraphic and sedimentological expression

Unconformity 1 (UC1) is identified in all six wells, although the time gap and stratigraphic expression varies significantly across the Måløy Slope. Towards the eastern basin margin, late Volgian marine mudstones (Draupne Formation) overlie late Oxfordian shallow marine clastics (Sognefjord Formation), suggesting an unconformity spanning *ca*.11 Myr (36/7-2; Figs 5A and 6; see also Table 1; cf. seismic expression of the unconformity described in section 4.1.2). Further west, in the footwall of the Gjøa Fault Zone, UC1 is underlain by Middle Bathonian shallow marine clastics (Fensfjord or Krossfjord formations), and overlain by Early Volgian (35/9-2 and 36/7-3) or early Hauterivian, deep-marine mudstones (35/9-1 and 36/7-1) (Figs. 5 and 6; Table 1). These stratigraphic relationships indicate that the time represented by the unconformity defined by UC1 decreases downslope to c. 4 Myr, and that the unconformity formed in the middle Kimmeridgian-to-early Volgian. Locally, however, on the crests of rift-related structural highs located in the central part of the study area, UC1 merges with UC2 to form a composite unconformity. In this location, the entire pre-Late Jurassic succession is absent, and Caledonian metamorphic and late Aptian marine mudstone subcrop and onlap UC1, respectively (i.e. 35/9-3; Figs 5a and b and 6; see also Table 1), indicating a time gap of >250 Myr.

Core data from 36/7-1, which was drilled on the northern margin of an UC1-related canyon (Canyon C; Figs 5a, 5c and 7c), constrains the sedimentological expression of UC1 in a relatively downslope position. These data indicate that the Sognefjord Formation, which is composed of shallow marine sandstone (Figs 9 and 10), is sharply and erosionally overlain by a *ca*. 35 m thick interval of deep marine deposits that include: (i) sharp-based, massive, decimetre-scale beds of fine-to-medium grained, turbidite sandstone, which locally are dewatered; (ii) metre-thick beds of very finely-laminated slope mudstone, which contain current-ripple laminated siltstones and very fine-grained sandstone; and (iii) thin beds of very poorly-sorted, and locally conglomeratic, muddy sand debrites (Figs 9 and 11). High gamma-ray values (>80 API) in well-log data and lithological observations from cuttings data indicate the upper part of the canyon-fill, above UC1 but below UC2, is dominated by hemipelagic mudstone (2018-2125 m; Figs 5a, 5c and 9). Well-log and cuttings data from other uncored wells indicate mudstone dominates the canyon-fill (35/9-1 and 35/9-2; Fig. 5); the exception to this is 36/7-3, which is drilled slightly north of the axis of Canyon 1B and that documents several 5-30 m thick, sharp-based, presumably turbidite sandstone-dominated packages (e.g. 2765-2795 m; Fig. 5B) separated by mudstone. Despite being relatively thin, these sandstone-rich packages overlie unconformities that define significant time gaps (up to 8.5 Myr; Fig. 6) that are as long as the major, slope-wide, canyon-defining unconformities (i.e. UC1, 2 and 3; Fig. 6 and Table 1).

4.1.2. Seismic expression and basin-scale morphology

East of the Måløy Fault, UC1 is represented by a relatively high-amplitude, laterally continuous reflection that is conformable with underlying and overlying reflections (Figs 7a-b). Given that borehole data indicate a time gap of *ca*. 11 Myr along the basin margin, the lack of seismic-scale incision suggests UC1 is, at least in this position, related to a period of stratigraphic condensation and/or non-deposition, perhaps related to downslope sediment bypass (see below). In contrast, downslope, west of the Måløy Fault, UC1 defines a prominent erosion surface, along which four broadly ESE-trending canyons are developed (labelled 1A-D; Figs 7C-E and 13A). The heads of the southernmost canyons are located in the immediate hangingwall of the Måløy Fault (C and D; Fig. 13A). Although the heads of the northernmost canyons are not preserved due to erosion beneath the younger canyons associated with UC2, we infer they were located in the immediate hangingwall of the Måløy Fault (A and B; Fig. 13A). These canyons are up to 700 m deep and 9 km wide, typically widening downslope to the west (canyons C and D; Fig. 13A). The canyons are flat-bottomed, display 'U'-shaped geometry in cross-section, and their margins are smooth and dip up to 5° (Fig. 7C-E). The two northern canyons extend outside of the area of seismic data coverage, thus are at least 35 km long. In the immediate footwall of the Gjøa Fault, UC1-related canyons and their fill are eroded and thus variably preserved beneath younger, UC2- and UC3-related canyons (i.e. Canyon 1C in Fig. 7E; see also Fig 13A).

The four UC1-related canyons trend broadly perpendicular to the majority of rift-related faults on the Måløy Slope (Fig. 13A). However, these canyons are offset by the northern and southern segments of the Gjøa Fault, in addition to a number of smaller faults located in its hangingwall (Fig. 4). We note that the magnitude of base-canyon incision increases into the footwalls of the faults whereas the canyon fill thickness decreases (i.e. footwall of GFN in Fig. 4).

4.1.3. Origin and evolution

Using seismic reflection and borehole data from the northern Måløy Slope and Slørebotn Sub-basin, Jackson et al. (2008) and Sømme et al. (2013) describe broadly 'Late Jurassic' canyons of comparable geometry and dimension to those associated with UC1. As such, we interpret UC1 to represent the along-strike continuation of the Upper Jurassic Unconformity (UJUNC) as previously defined elsewhere along the margin. We thus infer that UC1-related slope canyons are genetically related to those developed further north, suggesting slope incision occurred along an at least 200 km strike length of the southern Norwegian margin during the Late Jurassic.

Based on observations from modern and ancient deep-marine systems, three principal mechanisms are typically cited to explain the formation of submarine slope canyons: (i) marine flooding of incised-valleys eroded into a previously subaqueous shelf and cut in a subaerial setting by fluvial processes during a preceding period of relative sea-level fall (e.g. Van Wagoner, 1995); (ii)

retrogressive failure of a slope in a fully subaqueous setting (e.g. Twichell & Roberts, 1982; McGregor et al., 1982; Farre et al., 1983); and (iii) incision of a slope by downslope-eroding sediment gravity flows in a fully subaqueous setting (e.g. Spinelli & Field, 2001; Jobe et al., 2011; Lonergan et al., 2013; Prélat et al., 2015; Lai et al., 2016). Given their markedly different modes of formation, and the environments in which they operate, the applicability of these mechanisms to the formation of the UC1 (and younger) canyons can be tested using observations from our geophysical and geological data.

UC1 canyons incised Upper Jurassic shallow marine rocks. Based on this stratigraphic relationship it is possible that UC1 represents a sequence boundary, and that canyons thus initiated as fluvially-cut valleys incised into the shelf in response to a relative fall in sea level. This interpretation implies the deep-marine rocks filling the canyons were deposited during the subsequent period of marine flooding, which eventually established deep-marine conditions across much of the Norwegian margin. However, we do not think that the UC1 canyons formed due to this process for the following five reasons: (i) the Late Jurassic was a time of eustatic sea-level rise, and it seems unlikely that a large magnitude fall in relative sea-level, due to local tectonic uplift, would have occurred during a time of crustal extension and rapid fault-driven subsidence; (ii) the canyons are developed within a fully marine sequence documenting a net increase in water depth with time; although core data are lacking in some boreholes, we have no evidence that UC1 was associated with subaerial exposure of the slope; (iii) canyons of similar dimensions are not observed at the same stratigraphic level elsewhere within the rift and, although some Upper Jurassic fault blocks were locally exposed and eroded, these are related to the formation of relatively narrow (<2 km), strike discontinuous (up to a few tens of km) 'islands' located in the footwalls of large, rift-related faults (e.g. Nøttvedt et al., 2000; Roberts et al., 2019); (iv) the canyons are significantly deeper than (incised) valleys typically formed in response to base-level fall; and (v) the magnitude of erosion increases downslope along UC1-related canyons; this is contrary to that predicted by an incised-valley model. It thus seemly highly likely that UC1 canyons formed in a submarine rather than subaerial setting, in response to mechanism (ii) or (iii).

When considering mechanisms (ii) (i.e. retrogressive failure of a submarine slope) and (iii) (i.e. incision of a submarine slope by downslope-eroding sediment gravity flows), we note that similar age strata subcrop UC1 across the slope, despite the surface presently displaying a pronounced westward dip (i.e. Late Jurassic; Figs 4A and 6; see also Table 1). This observation suggests only minor tectonic relief was generated at this time; more specifically, this implies that most of the westwards tilting of the Måløy Slope occurred later and that retrogressive slope failure played only a minor role in canyon initiation. This interpretation is consistent with the observation that pre-UC1 deposits are broadly tabular and do not thicken across slope-perpendicular faults, suggesting limited tectonic activity at this time.

Slope incision and canyon development may thus have occurred due to the input of erosive sediment gravity flows, perhaps sourced from basin-margin clastic systems like the stratigraphically older Sognefjord Delta (e.g. Dreyer et al., 2005; Patruno et al., 2014; 2015). This interpretation is

consistent with data from borehole 36/7-3, which indicate the input of turbidites may be associated with significant time gaps (up to 8 Myr), perhaps related to seabed erosion and sediment bypass (e.g. Stevenson et al., 2015). Furthermore, borehole and seismic data from 36/7-2 indicate that the fault-controlled shelf was possibly an area of sediment bypass for up to 11 Myr; these sediments may then have entered the canyons at their headwalls, immediately downdip of the Måløy Fault (Fig. 13A). Irrespective of the mechanism driving canyon development, the slope was tectonically active during the Late Jurassic as indicated by the magnitude of incision increasing into the footwalls of slope-perpendicular normal faults, which are locally associated with across-fault changes in stratigraphic thickness (i.e. between 36/7-3 and 35/9-3 and 36/7-1 and 35/9-1; Fig. X).

4.2. Unconformity 2 (UC2)

4.2.1. Stratigraphic and sedimentological expression

Like UC1, the time gap represented by UC2 varies markedly across the Måløy Slope, with the unconformity locally forming a composite surface with older (UC1) and younger (UC3) unconformities. Upslope, towards the eastern basin margin, in the immediate hangingwall of the Øygarden Fault Zone, early Aptian deep-marine strata directly overlie early Barremian deep-marine strata across UC2, which represents an unconformity with a duration of *ca*. 6.5 Myr (36/7-2; Figs 5A and 6; see also Table 1). Downslope, in the immediate hangingwall of the Gjøa Fault Zone and near the axis of a large canyon, late Aptian deep-marine strata directly overlie late Barremian deep-marine strata across UC2, thereby indicating an unconformity of *ca*. 18 Myr (36/7-3, on the northern flank of Canyon 1C; Figs 5A, 5B and 6; see also Table 1). We observe a slightly longer duration unconformity of *ca*. 21.5 Myr on the southern margin of the same canyon, defined by the juxtaposition of Early Hauterivian deep-marine strata above late Oxfordian-Kimmeridgian deep-marine strata (36/7-1; Fig. 6; see also Table 1). Slightly further downslope to the west, in the immediate footwall of the northern segment of the Gjøa Fault Zone, UC2 cuts down to merge with UC1, forming part of a composite unconformity documenting a time gap of at least 300 Myr; here, late Aptian deep-marine strata directly overlie metamorphic rocks (i.e. 35/9-3; Figs 5A and 6; see also Table 1). UC2 also forms a composite unconformity with UC3 further downslope to the south, in the immediate footwall of southern segment of the Gjøa Fault. Here, lower Turonian and late Aptian deep-marine strata are juxtaposed, recording an unconformity of *ca*. 6 Myr (i.e. 35/9-2; Figs 5A and 6; see also Table 1). In summary, we find the magnitude of erosion associated with UC2 increases downslope. However, it must be noted that UC2 typically incises down to broadly the same stratigraphic level within the early Barremian to earliest Aptian, with spatial variations in the associated unconformity reflecting onlap of progressively younger strata upslope (i.e. eastward); for example, late Albian and early Turonian strata overlie UC2 in distal areas, whereas early Aptian and early Albian overlie UC2 in proximal areas (Fig. 6; see also Table 1).

Given the minimum unconformity documented, we interpret UC2 formed over a *ca*. 2 Myr period in the early Aptian (i.e. youngest rocks of Early Aptian age below UC2 in 35/9-2; oldest rocks of Early Aptian age above UC2 in 36/7-2).

Due to a lack of core data in the Lower and Upper Cretaceous and in basement rocks, we constrain the stratigraphic expression of the UC2 using only wireline log and cuttings data. These data indicate that, where UC2 forms a discrete stratigraphic surface separate from UC1 and UC3, its stratigraphic expression is subtle, with deep-marine mudstone (Rødby Formation) directly overlain by deep-marine marl (Åsgard Formation). As a result of this stratigraphic juxtaposition, UC2 has no distinct expression on wireline log data (Fig. 5). However, in the north of the study area, where a large canyon developed along UC2, thick (up to 100 m) packages of turbidite sandstone occur in the Rødby Formation (i.e. Canyon 2G in 36/7-3; Fig. 5A and 5B) (Martinsen et al., 2005). Biostratigraphic data do not resolve erosion-related unconformities at the bases of these sandstone-rich packages (Fig. 6).

4.2.2. Seismic expression and basin-scale morphology

On the proximal, eastern part of the Måløy Slope, east of the Måløy Fault, UC2 is expressed as a relatively low-amplitude, laterally continuous reflection that is conformable with underlying and overlying reflections (Fig. 7A), or that truncates underlying reflections basinward at a relatively low angle (Fig. 4A). Given that borehole data indicate an unconformity of *ca*. 6.5 Myr along the basin margin, the lack of seismic-scale incision suggests UC2 is, at least in this position, related to a period of stratigraphic condensation and/or non-deposition, perhaps related to downslope sediment bypass (see below). In contrast, further downslope to the west, UC2 forms a prominent erosion surface, along which four canyons are developed (Figs 7B-E and 13B). Constraining the position of the canyon heads is problematic due to deep incision below younger, UC3-related canyons; however, we infer the heads of UC2-related canyons were located either in the immediate hangingwall or the immediate footwall of the Måløy Fault (Fig. 13B). UC2 canyons are straight, and trend SE or SSE, thus are slightly oblique to those developed along UC1 (cf. Figs 13A and 13B). The canyons are 'V'- or 'U'-shaped in cross-section (margins dips of up to 5°), and are <2 km wide and up to 400 m deep, thus are generally narrower and shallower than those along UC1. UC2 canyons abruptly widen and display less relief downslope to the NW, passing into a low-relief erosion surface lacking canyons (Figs 7A-D). However, further downslope, in the footwall of the Gjøa Fault, the magnitude of erosion along UC2 increases dramatically and a very wide (up to 10 km wide), deep (c. 550 m) canyon is developed (Canyon 2G; penetrated by 35/9-3; Fig. 7E and D; see also Figs 5A-B and 13B). A second canyon, which is at least 10 km wide, c. 320 m deep and superimposed on an underlying, UC1-related canyon, is developed in the south of the study area (Canyon 2F, superimposed on Canyon 1D; Figs 7E and 13B).

The four canyons developed along UC2 trend broadly perpendicular to the majority of rift-related faults (Fig. 13B). Furthermore, the majority of normal faults on the Måløy Slope tip-out beneath

UC2 (Fig. 4), although the depth of incision along its base increases markedly across the Gjøa Fault, such that a canyon is present in the footwall of this structure (Figs 7E and 13B). UC2 is also locally offset, by up to 20 ms TWT, across normal faults adjacent to the Gjøa and Måløy fault zones (Fig. 4).

4.2.3. Origin and evolution

UC2 document a second period of slope incision, forming over *ca*. 6.5 Myr in the early Albian, after a *ca*. 30 Myr period of UC1 canyon filling and broader slope onlap. Based on the criteria discussed above, and given its development within a fully deep-marine succession, it seems likely that UC2 also formed subaqueously, due to either slope failure and/or erosion by sediment gravity flows. Furthermore, the occurrence of a moderate unconformity (*ca*. 6.5 Myr) along the basin margin, coupled with a lack of seismic-scale erosion, implies that, like UC1, UC2 was not associated with major erosion of the shelf, but rather a protracted period of sediment bypass to the slope. The eastward extension of UC2 canyons upslope of those developed along UC1 (i.e. slightly in to the footwall of the Måløy Fault) suggest the Måløy Fault System was not as active and may have become inactive by the early Albian, resulted in a weakly fault-controlled shelf edge, and allowing canyons to propagate landward.

Downslope, UC2 canyons incised into and presumably reworked sediments basinward previously contained within UC1 canyons. Furthermore, although most slope-normal, rift-related faults became inactive by the time UC2 formed, a marked increase in the depth of incision at the base of a UC2-related canyon across the northern segment of the Gjøa Fault System, suggests this structure continued to be active into the Aptian, enhancing incision along the canyon base. Furthermore, local amalgamation of UC2 and UC3 in the footwall of the Måløy Fault System suggests this structure was also active at this time.

4.3. Unconformity 3 (UC3)

4.3.1. Stratigraphic and sedimentological expression

UC3 is similar to the older unconformities in that its stratigraphic expression varies across the Måløy Slope. On the upper slope, in the immediate hangingwall of the Øygarden Fault Complex, UC3 locally merges with older (including UC2) and younger unconformities, capping and being overlain by late Albian and early Eocene deep-marine deposits, respectively; this defines a time gap of *ca*. 155 Myr (i.e. 36/7-2; Figs 6 and 7A; see also Table 1). Downslope to the west, UC3 is typically characterised by a correlative conformity defining a transition from Albian to Cenomanian deep-marine mudstone (i.e. 35/9-3, 36/7-1, 36/7-3; Figs 5 and 6; see also Table 1). The exception to this occurs in 35/9-2, in the immediate footwall of the Gjøa Fault System, where UC3 merges with UC2, thereby defining an unconformable upward transition from early Aptian deep-marine mudstone to early Turonian deep-

marine marl, and a time gap of *ca*. 20 Myr (Figs 5A and 6; see also Table 1). Constraining the age of UC3 is difficult; both 36/7-2 and 35/9-2 penetrate UC3 where it forms part of a composite unconformity, whereas other wells penetrate it in a relatively distal position where it defines a correlative conformity (35/9-3, 36/7-1, 36/7-3). 35/9-2 at least constrains the possible oldest (i.e. early Albian) and youngest (i.e. early Turonian) age, and the maximum time gap (i.e. *ca*. 20 Myr) associated with UC3. However, UC3 must be younger than UC2 (early Aptian), suggesting it defines an unconformity of <20 Myr duration.

4.3.2. Seismic expression

On the upper slope, on the northern part of the terrace bound by the Måløy Fault and the Øygarden Fault Complex, UC3 is typically expressed as a major angular unconformity; however, as described above, borehole data indicate that, on the southern part of this terrace, UC3 forms a composite unconformity with the much younger, base Pleistocene unconformity (Fig. 7A) (Martinsen et al., 2005). Slightly further downslope, UC3 is strongly erosional and represented by a discrete surface that marks the development of at least five canyons (Figs 7A and 7B), which pass north-westwards into a conformable, canyon-free surface on the lower slope (Fig. 13C). These upper slope canyons are relatively straight and trend E or SE, slightly oblique to those that developed slightly further downslope along UC2, and sub-parallel to those located even further downslope in UC1 (cf. Fig. 13C with Figs 13A and B). In cross-section, the UC3-related canyons have distinct 'V'-shaped geometries, and are up to 300 m deep, 3 km wide and have relatively steep margins (up to 10°). The observation that UC3 becomes confirmable downslope is consistent with observations from borehole data (see above).

UC3 is rarely offset by any rift-related faults (Fig. 4), implying the majority of these structures were inactive before the early Cenomanian. An exception to this is observed in the north-eastern corner of the study area, where UC3 is offset across a NW-SE-striking segment of the Måløy Fault (Fig. 4B).

4.3.3. Origin and evolution

UC3 documents a third and final period of slope incision, forming over a time period of a little under *ca*. 20 Myr in the early Turonian, following a *ca*. 20 Myr period of UC2 canyon filling and broader slope onlap. We again infer that UC3 formed in a fully marine setting, given its development within deep-marine strata; as such, we suggest that, like UC1 and UC2, UC3 also formed subaqueously due to either slope failure and/or erosion by sediment gravity flows. Because base Pleistocene erosion removes the stratigraphic record of UC3 in the immediate hangingwall of the Øygarden Fault Zone, it is not clear if, like UC1 and UC2, UC3 dies-out onto the outer reaches of the contemporaneous shelf, and if it therefore associated with shelf bypass with limited erosion. However, it is clear that UC3 extended further upslope than the older canyons, and that it died-out downslope to the west into a

correlative conformity. These observations indicate continued landward propagation of the erosional surfaces and associated canyons, possibly in response to continued basin margin uplift, which tilted the slope and augmented erosion, and ongoing subsidence in the basin centre, which suppressed erosion and resulted in the formation of a correlative conformity.

6. Discussion

6.1. Stratigraphic context and the origin of submarine canyons

We used 3D seismic reflection and borehole data to describe the geometry and stratigraphic context of several large (up to 700 m deep and 9 km wide), slope-confined canyons preserved in late Mesozoic strata of the northern North Sea, offshore western Norway. These canyons record relatively protracted periods (c. 2-17 Myr) of slope degradation, separated by >10 Myr periods of deposition and slope accretion. The geometry and scale of these canyons, 100's metres deep and kilometres wide, are comparable to others described from outcrop and in seismic reflection data. Here we briefly describe some notable, relatively well-documented examples of submarine canyons, focusing on debates related to their stratigraphic context and genesis. We then consider the implications of these previous studies, in addition to our data presented here from the northern North Sea, for the slope evolution and stratigraphy.

The Wonoka canyons (Neoproterozoic; 570-550 Ma), South Australia are some of the largest and best-exposed, yet controversial canyons described from the rock record. The canyons are up to 1.5 km deep and 4 km wide, and thus of broadly comparable dimensions to those described here from the northern North Sea. The Wonoka canyons are also similar to the North Sea examples in that multiple (up to five) periods of incision and canyon formation are interpreted. In terms of their general stratigraphic context, most authors agree that the Wonoka canyons emanate from the lower, deep-water part of the Wonoka Formation and are underlain by deep-water rocks of the Bunyeroo Formation. The stratigraphic fill and thus origin of the Wonoka canyons remains highly contentious. For example, some authors interpret a deep-water canyon-fill succession, arguing the canyons formed in a fully submarine setting (e.g. von der Borch et al., 1982; Giddings et al., 2010). In contrast, other authors interpret the fill is fluvial-to-shallow marine (e.g. Eickhoff et al., 1988; von der Borch et al., 1989; Christie-Blick, 2001), arguing that the canyons formed as incised valleys (*sensu stricto*; Van Wagoner, 1995; Van Wagoner et al., 1998) that were filled during subsequent marine flooding (Christie-Blick et al., 1995). The latter model requires km-scale changes in relative sea-level, which lead these authors to invoke regional tectonic uplift or 'Messinian-style' drawdown of the marine waters. Giddings et al. (2010) recently rejected this interpretation, arguing that: (i) the basal conglomerate is marine, being deposited by strongly erosive, very coarse-grained sediment-gravity currents that carved the canyons; (ii) there is no evidence for subaerial exposure and related erosion of the canyon walls; and (iii) multiple large-

519 magnitude changes (i.e. several hundreds of metres) in relative sea-level, which are required to drive
520 incision and canyon formation, are highly unlikely.
521 The Baliste-Crécerelle canyon lies within the Upper Oligocene-Middle Miocene Mandarove
522 Formation, offshore Gabon (Wonham et al., 2000). The canyon is up to 4 km wide and 500 m thick,
523 slope-confined, and likely formed in a fully submarine setting over a >10 Myr; the scale and
524 stratigraphic context and of the Baliste-Crécerelle canyon is thus broadly similar to that documented
525 here from the northern North Sea. The base of the canyon is inferred to be diachronous, and six intra-
526 canyon erosion surfaces are identified within the canyon itself. These erosion surfaces, and the
527 stratigraphic packages they bound, record several phases of erosion and sediment bypass, and canyon
528 filling, possibly related to relative sea-level change and related changes in sediment supply from the
529 shelf. The Baliste-Crécerelle canyon is thought to have formed via retrogressive failure of the slope in
530 response to uplift of the African continent, with upslope propagation of the canyon heads eventually
531 cannibalizing the outer shelf. Erosion of the canyon base was augmented by sediment gravity-flows
532 derived from rivers or longshore drift.
533 Submarine canyons are also described using 3D seismic reflection data from the Ebro
534 Continental Margin, western Mediterranean (Bertoni & Cartwright, 2005). Although also slope-
535 confined, these Plio-Pleistocene canyons are smaller (0.5-2 km wide, 10-15 km long, and incise >50 m)
536 than those we describe from the northern North Sea. Several periods of canyon incision and filling are
537 identified within a relatively short period (i.e. 1.7 Myr, based on study interval duration indicated in
538 their fig. 5). The vertical extent of the canyons (>500 m), and their restriction to the upper-middle slope
539 to the base-of-slope of well-development clinoforms, is clear evidence for their fully submarine origin;
540 critically, their vertical extent is far greater than the magnitude of any eustatic sea-level falls
541 documented for the stratigraphic interval of interest (i.e. maximum of 100-150 m; Haq et al., 1987).
542 Their shelf-detached location, and their linear geometry, points to an origin by internally slope-driven
543 failure, with some contribution by erosion by shelf-sourced sediment gravity-currents (e.g. Bakley et
544 al., 1990; Robb, 1990; Pratson & Coakley, 1996).
545 This brief synthesis of some well-documented examples of exposed and buried examples of
546 submarine canyons indicate these features often form in fully deep-marine conditions, with limited or
547 no evidence for subaerial exposure. This observation, coupled with the recognition that slope incision
548 can occur at any stage in the relative sea-level cycle (e.g. Ebro; Bertoni & Cartwright, 2005), argues
549 against relative sea-level fall (or at least for complete subaerial exposure of the entire canyon length/dip
550 extent) as the main driver for canyon formation. Establishing the trigger for slope degradation remains
551 challenging. In the case of the Baliste-Crécerelle and, potentially, Wonoka canyons, margin-scale
552 tectonic uplift may have driven canyon formation; in the case of the northern North Sea examples we
553 describe here, slope tilting may also reflect tectonically-driven uplift of the basin margin *and* concurrent
554 basin subsidence, or simply faster subsidence in the basin axis compared to the flanks. In the case of
555 the Ebro Continental Margin, much smaller, more clearly slope-confined, ‘gully-like’ canyons may

have formed in response to downslope-eroding sediment gravity currents derived from the shelf edge, rather than major tectonic uplift and/or differential uplift (e.g. Spinelli & Field, 2001; Jobe et al., 2011; Lonergan et al., 2013; Prélat et al., 2015). The duration and pacing of degradational events likely reflects the factors controlling slope instability and incision; in the case of the northern North Sea and offshore Gabon, this is the pulsed nature of slope tilting, whereas in the Ebro example this would be the magnitude and timing of sediment delivery to the shelf edge and upper slope.

6.2. Stratigraphic development of submarine canyons

The stratigraphic record of submarine canyon formation, evolution, and abandonment is likely complex. However, our ability to read this record is poor because: (i) field exposures are spatially limited and contain the stratigraphic expression of only one or a few cycles of slope aggradation and degradation, and/or lack detailed chronostratigraphic constraints (e.g. Giddings et al., 2010; Hodgson et al., 2011, 2016); and (ii) bathymetric maps of the present seabed and/or near-seabed geophysical studies do not permit analysis of the longer-term (10^3-10^4 Myr) stratigraphic development of submarine canyons (e.g. McGregor et al., 1982; Twichell & Roberts, 1982; Spinelli & Field, 2001; Jobe et al., 2011; Lonergan et al., 2013). Using our high-quality 3D seismic reflection and borehole dataset, we are able to show that spatially varying patterns of canyon-related erosion and deposition lead to the development of a complex stratigraphic record. For example, slope-confined submarine canyons in the northern North Sea are underlain by erosion surfaces that pass downdip into correlative conformities. Updip towards the basin margin, canyon bases may pass into cryptic stratigraphic surfaces that document non-deposition and/or erosion, but which lack evidence for seismic-scale incision (e.g. UC1). Furthermore, canyon-driven erosion, transport and (re)deposition leads to spatially complex patterns of sedimentation both above and downdip of the main areas of canyon incision. For example, after the canyon has formed, its downdip reaches are filled before more proximal areas, although in some cases the late-stage record is removed by younger canyons (see also Jackson et al., 2008). The transition from erosion to deposition in post-rift systems likely reflects the position of the 'fulcrum'; i.e. the approximate point around which the slope rotates. Areas updip of the fulcrum are experience and have their stratigraphic record principally controlled by relative sea-level fall and erosion, whereas those downdip by relative sea-level rise and deposition. However, this process will be highly time transgressive and the location of the fulcrum may migrate, leading to a complex distribution of related deposits and their bounding surfaces (e.g. erosion and flooding surfaces). The ultimate distribution of erosion surfaces and overlying deposits are likely controlled by the rate of slope tilting and the magnitude of incision; in the case of the northern North Sea, there is a systematic migration of the canyons upslope towards the basin margin suggesting that the fulcrum of basinward tilt also migrated through time.

6.3. Implications for tectono-stratigraphic models of rifts

Marine rift-basin tectono-stratigraphic models indicate syn-rift sediment dispersal is intimately linked to the growth of normal faults (Gawthorpe & Leeder, 2000). During the early stage of rifting (so-called 'rift initiation'; *sensu* Prosser, 1993), relatively small volumes of sediment are derived from the low-relief scarps of numerous, short, low-displacement faults. In contrast, during the latter stages of rifting (so-called 'rift climax'; *sensu* Prosser, 1993), large volumes of sediment are sourced from the high-relief scarps formed in the footwalls of a few, long, large-displacement faults that accommodate the majority of ongoing rift-related strain. Strain localisation onto a few large faults causes increasing topographic segmentation of the rift and the formation of wider deeper graben and half-graben; as a result, sediments sourced from relatively large antecedent systems are trapped in proximal depocentres (rift-margin), leading to sediment starvation in more distal areas (rift-axis). We show that the formation of large canyons during the latter stages of rifting can result in significant and very spatially focused bypass of sediment to the rift-axis. These canyons represent major sediment conduits and may cross-cut major, still-active normal faults at a high angle establishing a transverse sediment transport route in contrast to earlier axial supply systems. The sediment volumes derived from consequent drainage systems forming in response to normal fault-driven uplift are thus relatively small, and the evolution to transverse sediment supply during the post-rift needs to be captured in future marine rift-basin tectono-stratigraphic models.

7. Conclusions

We integrated 3D seismic reflection and borehole data to determine the geometry and origin of ancient (Late Mesozoic) slope canyons, and their infills, on the Måløy Slope, offshore western Norway. We show that the initial phase of slope degradation (UC1) started in the Late Jurassic (late Kimmeridgian), during a period of rifting and active normal faulting. Two subsequent periods of slope degradation and canyon formation and infilling occurred during the post-rift in the Aptian-to-Albian (UC2) and Albian-to-Cenomanian (UC3). We constrain the timescales over which slope progradation and degradation occur, showing that the canyons record relatively protracted periods (c. 2-17 Myr) of slope degradation, separated by >10 Myr periods of deposition and slope accretion. Boreholes indicate that the canyons bases are defined by sharp, erosional surfaces, across which we observe an abrupt upward shift from shallow marine to deep marine (UC1), or deep marine to deep marine facies (UC2 and 3). The canyons are relatively straight, up to 700 m deep and 9 km wide on the upper slope, and die-out downdip onto the lower slope. All the canyons trend broadly perpendicular to, and crosscut most of, the rift-related Late Jurassic normal faults, although the oldest, late Kimmeridge canyons incise into the footwalls crests of structures that were still active at this time. The updip extent of the oldest, late Kimmeridgian canyons is defined by a fault-controlled shelf-edge, whereas the younger, Cretaceous canyons overstepped the now-inactive fault and incise the shelf. Slope degradation and canyon formation likely

reflects some combination of basinward tilting and over-steepening of this tectonically active rifted margin, augmented by slope incision by erosive sediment gravity-flows. We show that the geophysical and geological (i.e. stratigraphic) expression of slope degradation-related features (i.e. canyons) in the rock record is complex, and that their formation can drive a major reorganisation of rift-related drainage patterns and sediment dispersal; this is not currently predicted by existing marine rift-basin tectono-stratigraphic models.

Acknowledgments

Rob Gawthorpe, Paul Whipp, Rachel Kieft and Tor Sømme are thanked for discussions during the course of this study. Norsk Hydro ASA (now Equinor ASA) are thanked for funding this study by provision of a PhD studentship to AEM.

References

Adams, E.W., and Schlager, W., 2000. Basic types of submarine slope curvature. Journal of Sedimentary Research, 70, 814–828.

Asquith, D.O., 1970. Depositional topography and major marine environments, Late Cretaceous, Wyoming. AAPG Bulletin, 54, 184-1224.

Bakley, V.R., Kochel, R.C., Laity, J.E., and Howard, A.D., 1990) Spring sapping and valley network development. GSA Special Paper, 252, 235-265.

Bates, C.C., 1953. Rational theory of delta formation. AAPG Bulletin, 37, 2119–2162.

Bell, R.E., Jackson, C.A-L., Whipp, P.S. and Clements, B., 2014. Strain migration during multiphase extension: Observations from the northern North Sea. Tectonics, 33, 1936-1963.

Bertoni, C., and Cartwright, J., 2005. 3D seismic analysis of slope-confined canyons from the Plio-Pleistocene of the Ebro Continental Margin (Western Mediterranean). Basin Research, 17, 43-62.

Brown, A.R., 2011. Interpretation of three-dimensional seismic data. Society of Exploration Geophysicists and American Association of Petroleum Geologists.

Bugge, T., Tveiten, B. and Bäckström, S., 2001. The depositional history of the Cretaceous in the northeastern North Sea. In: Sedimentary Environments Offshore Norway — Palaeozoic to Recent (Eds Martinsen, O,J., Dreyer, T). Norwegian Petroleum Society Special Publications, 10, 279-291.

Christie-Blick, N., Dyson, I.A. and Von Der Borch, C.C., 1995. Sequence stratigraphy and the interpretation of Neoproterozoic Earth history. Precambrian Research, 73, 3-26.

Christie-Blick, N., Williams, G.E. and Gostin, V.A., 2001. Discussion on mantle plume uplift in the sedimentary record: origin of kilometre-deep canyons within late Neoproterozoic successions. Journal of the Geological Society, 158, 573-576.

Eickhoff, K.H., Von Der Borch, C.C. and Grady, A.E., 1988. Proterozoic canyons of the Flinders Ranges (South Australia): submarine canyons or drowned river valleys?. Sedimentary geology, 58, 217-235.

Figueiredo, J.J., Hodgson, D.M., Flint, S.S. and Kavanagh, J.P., 2013. Architecture of a channel complex formed and filled during long-term degradation and entrenchment on the upper submarine slope, Unit F, Fort Brown Fm., SW Karoo Basin, South Africa. Marine and Petroleum Geology, 41, 104-116.

Fraser, S.I., Robinson, A.M., Johnson, H.D., Underhill, J.R., Kadolsky, D.G.A., Connell, R., Johannessen, P., and Ravnås, R., 2003. Upper Jurassic. In: The Millennium Atlas: petroleum geology of the central and northern North Sea (Eds D. Evans, C. Graham, A. Armour and P. Bathurst), 157-189. Geological Society of London.

Fulthorpe, C.S., Austin Jr, J.A. and Mountain, G.S., 2000. Morphology and distribution of Miocene slope incisions off New Jersey: Are they diagnostic of sequence boundaries?. GSA Bulletin, 112, 817-828.

Færseth, R.B., 1996. Interaction of Permo-Triassic and Jurassic extensional fault-blocks during the development of the northern North Sea. Journal of the Geological Society, 153, 931-944.

Gabrielsen, R.H., Kyrkjebø, R., Faleide, J.I., Fjeldskaar, W., and Kjennerud, T., 2001. The Cretaceous post-rift basin configuration of the northern North Sea. Petroleum Geoscience, 7, 137-154.

Gawthorpe, R.L. and Leeder, M.R., 2000, Tectono-sedimentary evolution of active extensional basins. Basin Research, 12, 195–218.

Giddings, J.A., Wallace, M.W., Haines, P.W. and Mornane, K., 2010. Submarine origin for the Neoproterozoic Wonoka canyons, south Australia. Sedimentary Geology, 223, 35-50.

Gong, C., Wang, Y., Steel, R.J., Olariu, C., Xu, Q., Liu, X. and Zhao, Q., 2015. Growth styles of shelf-margin clinoforms: prediction of sand-and sediment-budget partitioning into and across the shelf. Journal of Sedimentary Research, 85, 209-229.

Helland-Hansen, W., Steel, R., Nakayama, K., and Kendall, C. G. St. C., 1989. Review and computer modelling of the Brent Group stratigraphy. In: Deltas: Sites and Traps for Fossil Fuels (Whateley, M.K.G. & Pickering, K.T., eds). Geological Society, London, Special Publication, 41, 253-267.

Hodgson, D.M., Di Celma, C.N., Brunt, R.L. and Flint, S.S., 2011. Submarine slope degradation and aggradation and the stratigraphic evolution of channel–levee systems. Journal of the Geological Society, 168(3), pp.625-628.

Hodgson, D.M., Kane, I.A., Flint, S.S., Brunt, R.L. and Ortiz-Karpf, A., 2016. Time-transgressive confinement on the slope and the progradation of basin-floor fans: Implications for the sequence stratigraphy of deep-water deposits. Journal of Sedimentary Research, 86(1), pp.73-86.

Hubbard, S.M., Covault, J.A., Fildani, A. and Romans, B.W., 2014. Sediment transfer and deposition in slope channels: deciphering the record of enigmatic deep-sea processes from outcrop. Bulletin, 126(5-6), pp.857-871.

Jackson, C.A.L., Barber, G.P. and Martinsen, O.J., 2008. Submarine slope morphology as a control on the development of sand-rich turbidite depositional systems: 3D seismic analysis of the Kyrre Fm (Upper Cretaceous), Måløy Slope, offshore Norway. Marine and Petroleum Geology, 25, 663-680.

Janocko, M., Nemec, W., Henriksen, S. and Warchoł, M., 2013. The diversity of deep-water sinuous channel belts and slope valley-fill complexes. Marine and Petroleum Geology, 41, pp.7-34.

Johannessen, E.P. and Steel, R.J., 2005. Shelf-margin clinoforms and prediction of deepwater sands. Basin Research, 17(4), pp.521-550.

Kane, I.A., Kneller, B.C., Dykstra, M., Kassem, A. and McCaffrey, W.D., 2007. Anatomy of a submarine channel–levee: an example from Upper Cretaceous slope sediments, Rosario Formation, Baja California, Mexico. Marine and Petroleum Geology, 24(6-9), pp.540-563.

Kjennerud, T. and Sylta, Ø., 2001. Application of quantitative palaeobathymetry in basin modelling, with reference to the northern North Sea. Petroleum Geoscience, 7, 331-341.

Koch, J.O., Frischbutter, A., Øygard, K. and Cater, J., 2018, January. The 35/9-7 Skarfjell discovery: a genuine stratigraphic trap, NE North Sea, Norway. In Geological Society, London, Petroleum Geology Conference series (Vol. 8, No. 1, pp. 339-354). Geological Society of London.

Kyrkjebø, R., Gabrielsen, R.H. and Faleide, J.I., 2004. Unconformities related to the Jurassic–Cretaceous synrift–post-rift transition of the northern North Sea. Journal of the Geological Society, 161, 1-17.

Lai, S.Y., Gerber, T.P. and Amblas, D., 2016. An experimental approach to submarine canyon evolution. Geophysical Research Letters, 43, 2741-2747.

Lonergan, L., Jamin, N.H., Jackson, C.A-L. and Johnson, H.D., 2013. U-shaped slope gully systems and sediment waves on the passive margin of Gabon (West Africa). Marine Geology, 337, 80-97.

Maier, K.L., Johnson, S,Y. and Hart, P. (2018) Controls on submarine canyon head evolution: Monterey Canyon, offshore central California. Marine Geology, 404, 24-40

Martinsen, O.J., Bøen, F., Charnock, M.A., Mangerud, G. and Nøttvedt, A., 1999, Cenozoic development of the Norwegian margin 60–64° N: sequences and sedimentary response to variable basin physiography and tectonic setting. In: Petroleum Geology of Northwest Europe: Proceedings of the 5th Conference (Eds A. J. Fleet, S.A.R. Boldy), 293-304. Geological Society of London.

Martinsen, O.J., Lien, T., & Jackson, C.A-L. (2005). Cretaceous and Palaeogene turbidite systems in the North Sea and Norwegian Sea Basins: source, staging area and basin physiography controls on reservoir development. In A.G. Dore, & B.A. Vining (Eds.), Petroleum geology: North-West Europe and global perspectives: proceedings of the 6th petroleum geology conference Vol. 2 of 2 (pp. 1147-1164). London: The Geological Society.

Mayall, M., Jones, E. and Casey, M., 2006. Turbidite channel reservoirs—Key elements in facies prediction and effective development. Marine and Petroleum Geology, 23(8), pp.821-841.

Neal, J. and Abreu, V., 2009. Sequence stratigraphy hierarchy and the accommodation succession method. Geology, 37(9), pp.779-782.

Patruno, S., Hampson, G.J., Jackson, C.A.L., Whipp, P.S., 2015. Quantitative progradation dynamics and stratigraphic architecture of ancient shallow-marine clinoform sets: a new method and its application to the Upper Jurassic Sognefjord Formation, Troll Field, offshore Norway. Basin Res. 27 (4), 412–452.

Patruno, S. and Helland-Hansen, W., 2018. Clinoforms and clinoform systems: Review and dynamic classification scheme for shorelines, subaqueous deltas, shelf edges and continental margins. Earth-Science Reviews, 185, 202-233.

Pirmez, C., Pratson, L.F., Steckler, M.S., 1998. Clinoform development by advection-diffusion of suspended sediment: modeling and comparison to natural systems. J. Geophys. Res. Solid Earth 103 (B10), 24141–24157.

Posamentier, H.W. and Vail, P.R., 1988. Eustatic controls on clastic deposition II—sequence and systems tract models. In: Sea-Level Changes – An Integrated Approach (Eds Wilgus; C.K., Hastings, B.S., Posamentier, H., Van Wagoner, J, Ross, C.A. Kendall, C.G.St.C). SEPM Special Publication, 42.

Pratson, L.F. and Coakley, B.J., 1996. A model for the headward erosion of submarine canyons induced by downslope-eroding sediment flows. GSA Bulletin, 108, 225-234.

Prosser, S., 1993. Rift-related linked depositional systems and their seismic expression. In: Tectonics and Seismic Sequence Stratigraphy (Eds G. D. Williams, A. Dobb). Geological Society, London, Special Publications, 71, 35-66.

Reeve, M.T., Bell, R.E. and Jackson, C.A.L., 2015. Origin and significance of intra-basement seismic reflections offshore western Norway. Journal of the Geological Society, 171(1), pp.1-4.

Rich, J.L., 1951. Three critical environments of deposition and criteria for recognition of rocks deposited in each of them. GSA Bull. 62, 1–20.

Robb, J.M. (1990) Groundwater processes in the submarine environment. GSA Special Paper, 252, 267-281.

Romans, B.W., Hubbard, S.M. and Graham, S.A., 2009. Stratigraphic evolution of an outcropping continental slope system, Tres Pasos Formation at Cerro Divisadero, Chile. Sedimentology, 56(3), pp.737-764.

Shepard, F.P., 1981. Submarine canyons: Multiple causes and long-time persistence, AAPG Bulletin, 65, 1062–1077.

Sømme, T.O. and Jackson, C.A.L., 2013. Source- to- sink analysis of ancient sedimentary systems using a subsurface case study from the Møre- Trøndelag area of southern Norway: Part 2–sediment dispersal and forcing mechanisms. Basin Research, 25, 512-531.

Sømme, T.O., Jackson, C.A.L. and Vaksdal, M., 2013. Source- to- sink analysis of ancient sedimentary systems using a subsurface case study from the Møre- Trøndelag area of southern Norway: Part 1–depositional setting and fan evolution. Basin Research, 25, 489-511.

Steckler, M.S., Mountain, G.S., Miller, K.G., Christie-Blick, N., 1999. Reconstruction of Tertiary progradation and clinoform development on the New Jersey passive margin by 2-D backstripping. Mar. Geol. 154 (1), 399–420.

Steel, R. and Ryseth, A., 1990. The Triassic—Early Jurassic succession in the northern North Sea: megasequence stratigraphy and intra-Triassic tectonics. Geological Society, London, Special Publications, 55(1), pp.139-168.

Steel, R.J., Olsen, T., 2002. Clinoforms, clinoform trajectory and deepwater sands. In: Armentrout, J.M., Rosen, N.C. (Eds.), Sequence Stratigraphic Models for Exploration and Production: Evolving Methodology, Emerging Models and Application Histories. GCS-SEPM Special Publication, pp. 367–381.

Sylvester, Z., Deptuck, M.E., Prather, B.E., Pirmez, C., O'Byrne, C., Mohrig, D., Van Hoorn, B. and Wynn, R.B., 2012. Seismic stratigraphy of a shelf-edge delta and linked submarine channels in the northeastern Gulf of Mexico. Application of the Principles of Seismic Geomorphology to Continental-Slope and Base-of-Slope Systems: Case Studies from Seafloor and Near-Seafloor Analogues: SEPM, Special Publication, 99, pp.31-59.

Sømme, T.O., Jackson, C.A.L. and Vaksdal, M., 2013. Source- to- sink analysis of ancient sedimentary systems using a subsurface case study from the Møre- Trøndelag area of southern Norway: Part 1–depositional setting and fan evolution. Basin Research, 25, 489-511.

Von der Borch, C.C., Smit, R. and Grady, A.E., 1982. Late Proterozoic submarine canyons of Adelaide Geosyncline, South Australia. AAPG Bulletin, 66, 332-347.

Van Wagoner, J.C., 1995. Overview of sequence stratigraphy of foreland basin deposits: terminology, summary of papers, and glossary of sequence stratigraphy. In: Sequence Stratigraphy of Foreland Basin Deposits: Outcrop and Subsurface Examples from the Cretaceous of North America (Eds J.C. Van Wagoner; G.T. Bertram). AAPG Memoir, 64, IX-XXI.

Van Wagoner, J.C., Posamentier, H.W., Mitchum, R.M.J., Vail, P.R., Sarg, J.F., Loutit, T.S. and Hardenbol, J., 1988. An overview of the fundamentals of sequence stratigraphy and key definitions. In: Sea-Level Changes – An Integrated Approach (Eds Wilgus, C.K., Hastings, B.S., Posamentier, H., Van Wagoner, J, Ross, C.A. Kendall, C.G.St.C). SEPM Special Publication, 42.

Wonham, J.P., Jayr, S., Mougamba, R. and Chuilon, P., 2000. 3D sedimentary evolution of a canyon fill (Lower Miocene-age) from the Mandorove Formation, offshore Gabon. Marine and Petroleum Geology, 17, 175-197.

Figure captions

Fig. 1. (A) Map showing the location of the study area (dashed black line) and major hydrocarbon exploration quadrants. Major structural elements, including key rift-related normal faults, are shown, as is the location of the cross-section shown in (B). Inset map shows the regional geographic location of the study area. CVG=Central Viking Graben; NVG=North Viking Graben; SG=Sogn Graben; LT=Lomre Terrace; UT=Uer Terrace; HP=Horda Platform; MS= Måløy Slope; TS=Tampen Spur; StF=Statfjord Fault; SnF=Snorre Fault; MFC=Mokkurkalve Fault Complex; SGF=Sogn Graben Fault; KF=Kinna Fault; VF=Vette Fault; GF=Gjøa Fault; GG=Gjøa Graben; MF= Måløy Fault; ØFC=Øygarden Fault Complex. (B) Schematic cross-section showing the regional geological setting of the study area.

Fig. 2. Stratigraphic column showing the interval of interest. We focus on the major Mesozoic unconformities (UC1-3). The maximum flooding surface (MFS) ('J-sequence') nomenclature is after Underhill & Partington (1993) (see also Fraser et al., 2003). The seismic horizon and stratal unit (SU) colour legend shown here applies to the geoseismic profiles in Figs 4 and 7, and the synthetic seismograms in Fig. 8.

Fig. 3. (A) Time-structure map of the top basement seismic horizon, illustrating the rift-related structure of the study area. Locations of seismic profiles in Figs 4a-b and 7a-e are shown, as are the locations of key boreholes used in the study (see Figs 5, 6, 8 and 9-12). (B) Dip-map of the top basement time-structure map highlighting the key structural elements within the study area. The locations of

887 stratigraphic correlations in Fig. 5 are shown. GFN= Gjøa Fault North; GFS= Gjøa Fault South; MFN=
888 Måløy Fault North; MFS= Måløy Fault South; ØFC=Øygarden Fault Complex; GG= Gjøa Graben.
889
890 **Fig. 4.** (A) SE- and (B) SSE-trending seismic (above) and geoseismic (below) profiles across the study
891 area, showing the rift-related structure of the deep part of the Måløy Slope, and the structural and
892 stratigraphic context of the Mesozoic unconformities (UC1-3; see Fig. 2). Abbreviations for the
893 structural elements is in Fig. 3. The locations of intersecting seismic and geoseismic profiles in Fig. 7
894 are shown. 1C, 2G, etc, refer to specific unconformity-related canyons referred to in the text and
895 highlighted on the stratigraphic correlations shown in Fig. 5.
896
897 **Fig. 5.** (A) Regional stratigraphic correlation between key wells on the Måløy Slope showing the overall
898 structural and stratigraphic context of the Mesozoic unconformities (UC1-3; see Fig. 2). (B) Local
899 stratigraphic correlation between wells located in the footwall (35/9-3) and hangingwall (36/7-3) of the
900 GFN. (C) (B) Local stratigraphic correlation between wells located in the footwall (35/9-1) and
901 hangingwall (36/7-1) of the GFS. The overall lithology of the material eroded into by and filling the
902 Mesozoic canyons, and overlying with intra-canyon bypass surfaces, is shown. Stars on the left-hand
903 side of the boreholes indicate the locations of the biostratigraphic samples that constrain the
904 chronostratigraphic framework and surface correlation. Hachured areas in the 'chronostratigraphy'
905 column indicate areas lacking age diagnostic fauna. The geometry of UC1-related canyons between
906 35/9-1 and 35/9-2, and in the immediate hangingwall of the GFS and GFN, is constrained by
907 observations from seismic reflection data (e.g. Figs 4 and 7). Location of correlation shown in Fig. 3B.
908 1C, 2G, etc, refer to specific unconformity-related canyons referred to in the text and highlighted on the
909 seismic profiles shown in Figs 4 and 7.
910
911 **Fig. 6.** Wheeler-style diagram showing the stratigraphic context and expression of Mesozoic
912 unconformities on the Måløy Slope. Stratigraphically continuous sections are shown in white; hachured
913 areas indicate major time gaps, some of which define seismic-scale canyons (see Figs 4 and 7). Error
914 bars are based on uncertainties related to biostratigraphic sample spacing (see stars in Fig. 5). See text
915 for full discussion.
916
917 **Fig. 7.** N-trending seismic (above) and geoseismic (below) profiles across the study area, showing the
918 rift-related structure of the deep part of the Måløy Slope, and the structural and stratigraphic context of
919 the Mesozoic unconformities (UC1-3; see Fig. 2). (A) is located in the most proximal/upslope position;
920 (E) is located in the most distal/downslope position. Abbreviations for the structural elements is in Fig.
921 3. The locations of intersecting seismic and geoseismic profiles in Fig. 4 are shown. 1C, 2G, etc, refer
922 to specific unconformity-related canyons referred to in the text and highlighted on the stratigraphic
923 correlations shown in Fig. 5.

Fig. 8. Synthetic seismograms for (A) 36/7-3 and (B) 36/7-1. See Figs 3-5 and 7 for location of wells. The overall lithology of the material eroded into by and filling the Mesozoic canyons is shown. See Fig. 2 for colour legend.

Fig. 9. Core description from 36/7-1, showing the sedimentary facies and depositional environment immediately below and above UC1. Note the sharp upward transition from shallow- (shoreface) to deep-marine (slope canyon) facies. FS=flooding surface; RS=regressive surface See text for full description. See Figs 3 and 5 for location of the borehole. Locations of photos shown in Figs 11 and 12 are labelled.

Fig. 10. Core photograph showing the sedimentary facies and depositional environments encountered below UC1 in 36/7-1. Note the upwards transition from highly bioturbated, silt-rich, lower shoreface sandstone to bioclastic, medium-grained, upper shoreface sandstone; the contact between these two facies is sharp, occurring across a regressive surface (RS). Location of photo shown in Fig. 9.

Fig. 11. Core photograph showing the sedimentary facies and depositional environments encountered immediately below and above UC1 in 36/7-1. Note the sharp upward transition from shallow- (shoreface) to deep-marine (slope canyon) facies. See text for full description. Location of photo shown in Fig. 9.

Fig. 12. Photographs showing details of the deep-marine facies encountered in the UC1-related canyon-fill succession. (A) deformed, thin-bedded, mud clast-rich, fine-grained turbidites, erosively overlain by mud- and clast-rich debrite; (B) thin-bedded, very fine-grained turbidites, erosively overlain by sand- and clast-rich debrite; (C) strongly deformed, thin- and thick-bedded turbidites; (D) sandy conglomerate containing abundant extrabasinal clasts.

Fig. 13. Isochrons (time-thickness maps) (left) and sketches (right) illustrating the geometry and distribution of Mesozoic unconformity-related canyons on the Måløy Slope. (A) SU3 (related to UC1); (B) SU4 (related to UC2); and (C) SU5 (related to UC3). Solid red lines=mapped canyon thalwegs; dashed red lines= inferred canyon thalwegs. See text for full discussion.

Table 1. Table showing the stratigraphic context and sedimentological expression of Mesozoic unconformities on the Måløy Slope.

Fig. 1

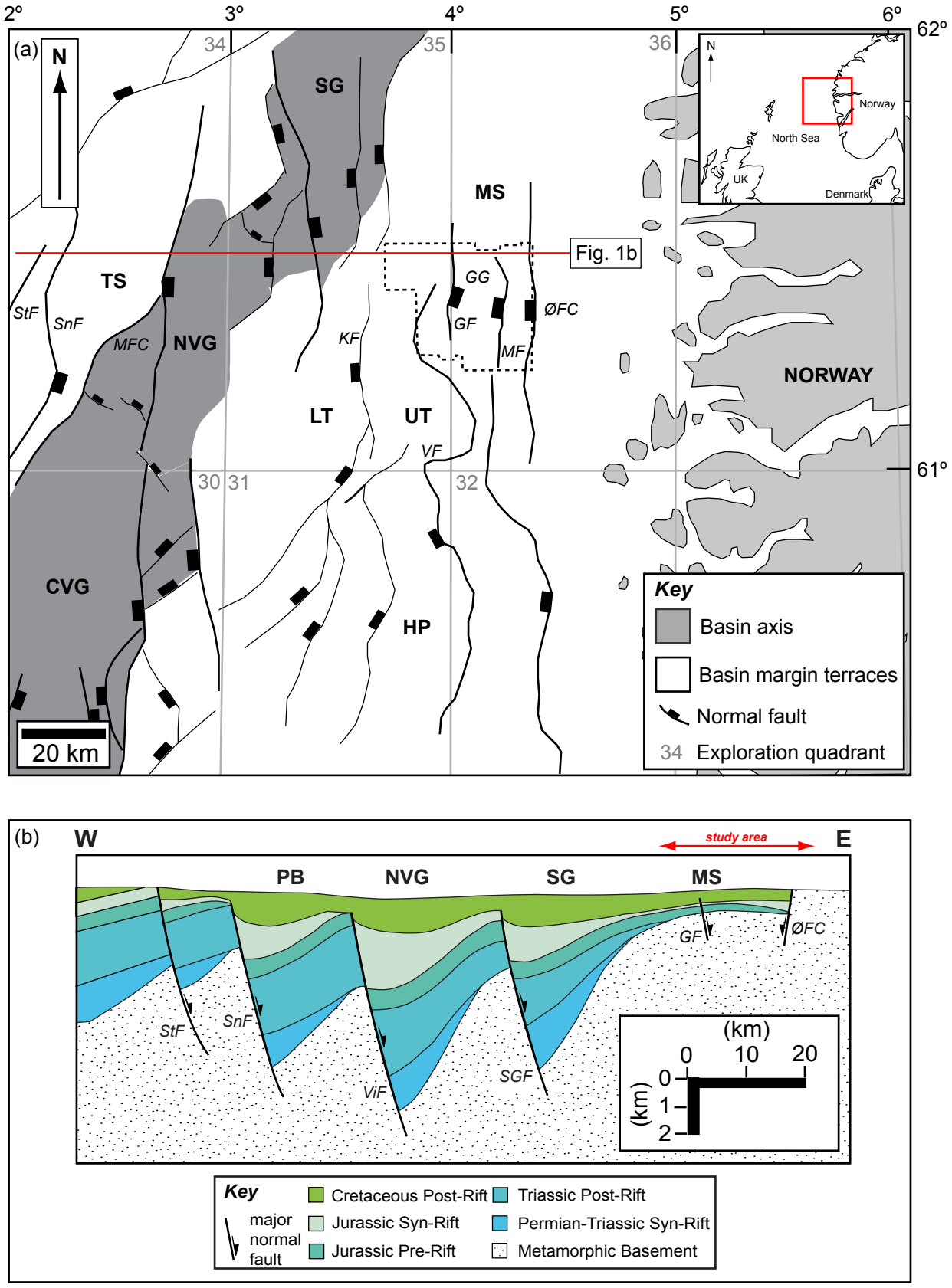
(a)
N
2º
3º
4º
5º
6º
62º
61º
34
35
36
30
31
32
SG
MS
TS
NVG
CVG
LT
UT
HP
NORWAY
StF
SnF
MFC
KF
GG
GF
MF
ØFC
VF
Fig. 1b
20 km
N
Norway
North Sea
UK
Denmark
Key
Basin axis
Basin margin terraces
Normal fault
34 Exploration quadrant
(b)
W
E
study area
PB
NVG
SG
MS
StF
SnF
ViF
SGF
GF
ØFC
(km)
0
10
20
0
1
2
Key
major normal fault
Cretaceous Post-Rift
Jurassic Syn-Rift
Jurassic Pre-Rift
Triassic Post-Rift
Permian-Triassic Syn-Rift
Metamorphic Basement

Fig. 2

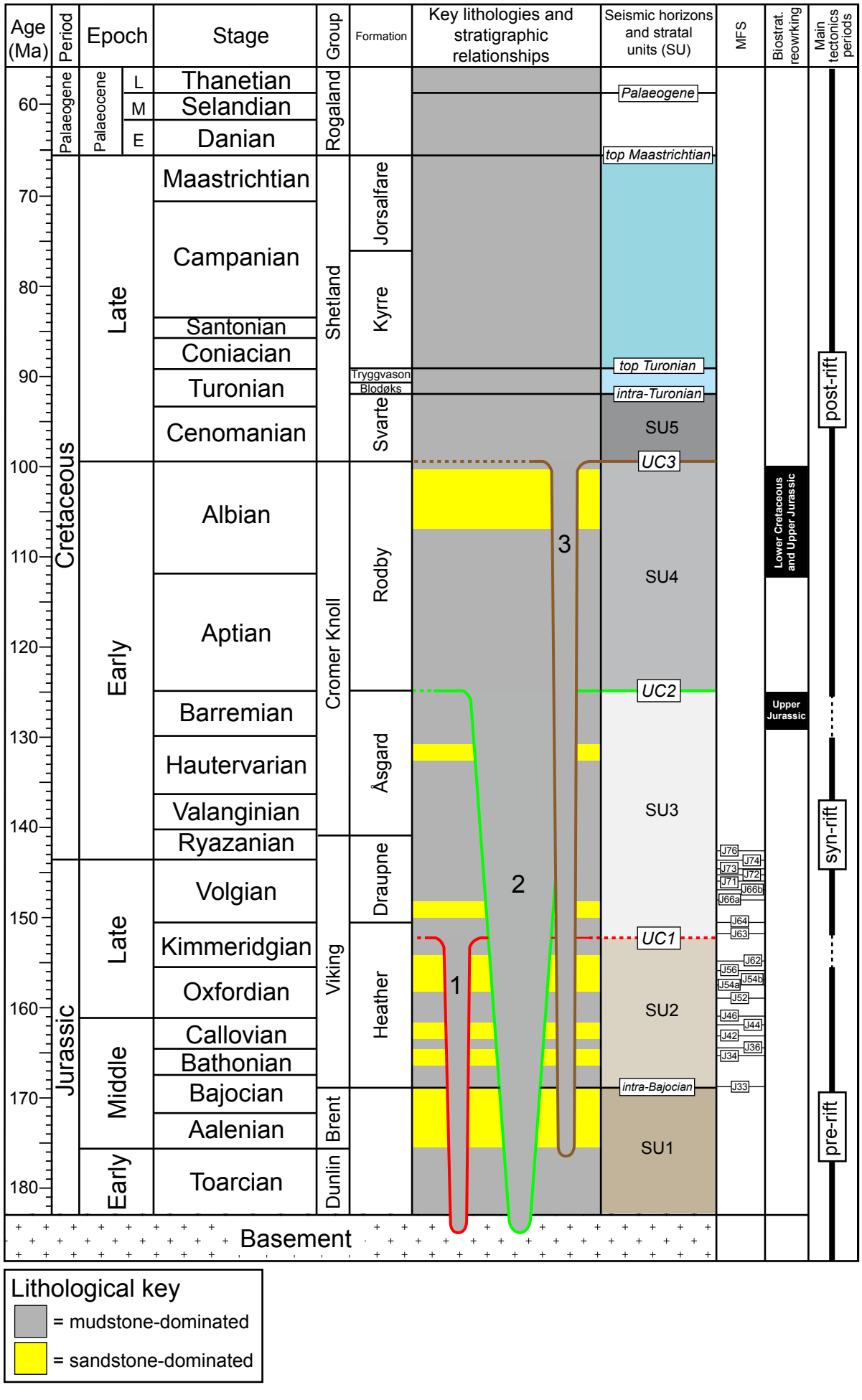
Age (Ma)
Period
Epoch
Stage
Group
Formation
Key lithologies and stratigraphic relationships
Seismic horizons and stratal units (SU)
MFS
Biostrat. reowrking
Main tectonics periods
Palaeogene
Cretaceous
Jurassic
Palaeocene
L
M
E
Late
Early
Middle
Thanetian
Selandian
Danian
Maastrichtian
Campanian
Santonian
Coniacian
Turonian
Cenomanian
Albian
Aptian
Barremian
Hautervarian
Valanginian
Ryazanian
Volgian
Kimmeridgian
Oxfordian
Callovian
Bathonian
Bajocian
Aalenian
Toarcian
Rogaland
Shetland
Cromer Knoll
Viking
Brent
Dunlin
Jorsalfare
Kyrre
Tryggvason
Blodøks
Svarte
Rodby
Åsgard
Draupne
Heather
Palaeogene
top Maastrichtian
top Turonian
intra-Turonian
SU5
UC3
SU4
UC2
SU3
UC1
SU2
intra-Bajocian
SU1
1
2
3
Basement
Lower Cretaceous and Upper Jurassic
Upper Jurassic
post-rift
syn-rift
pre-rift
Lithological key
= mudstone-dominated
= sandstone-dominated

Fig. 3

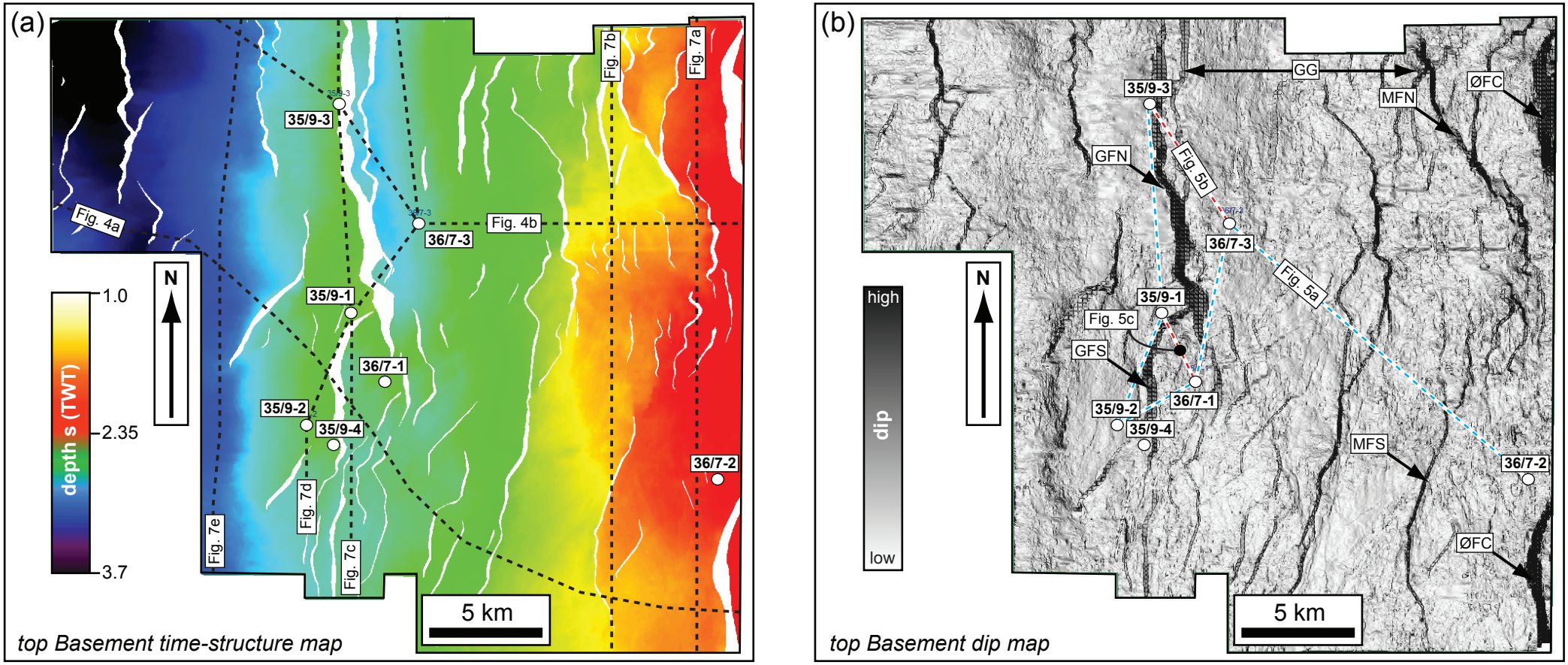
(a)
35/9-3
36/7-3
35/9-1
36/7-1
35/9-2
35/9-4
36/7-2
Fig. 4a
Fig. 4b
Fig. 7a
Fig. 7b
Fig. 7c
Fig. 7d
Fig. 7e
depth s (TWT)
1.0
2.35
3.7
N
5 km
top Basement time-structure map
(b)
GG
MFN
ØFC
GFN
Fig. 5b
Fig. 5a
Fig. 5c
GFS
MFS
high
dip
low
N
5 km
top Basement dip map

Fig. 4

(a)

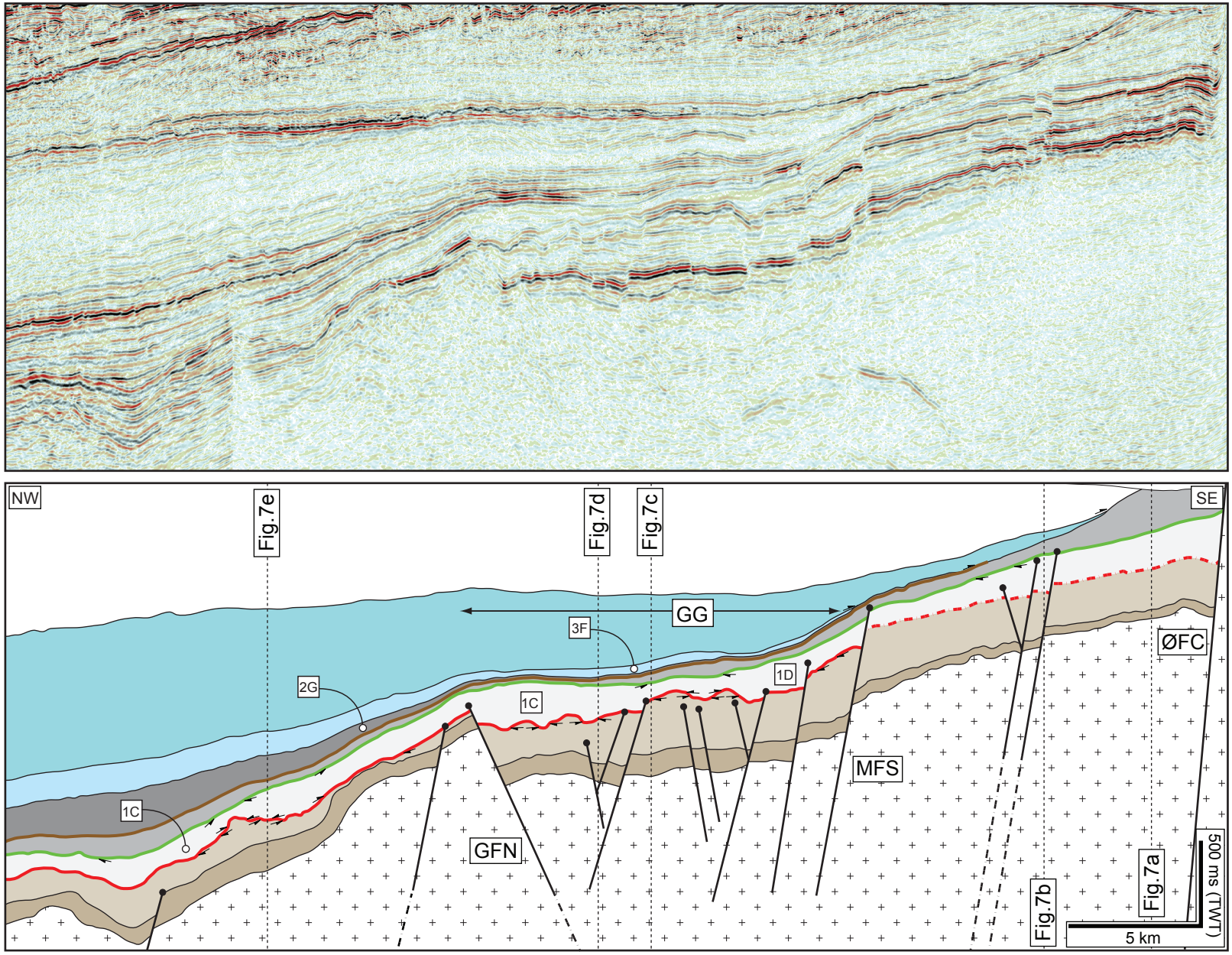
NW
SE
Fig.7e
Fig.7d
Fig.7c
GG
3F
2G
1C
1D
ØFC
MFS
GFN
1C
Fig.7b
Fig.7a
500 ms (TWT)
5 km

Fig. 4

(b)

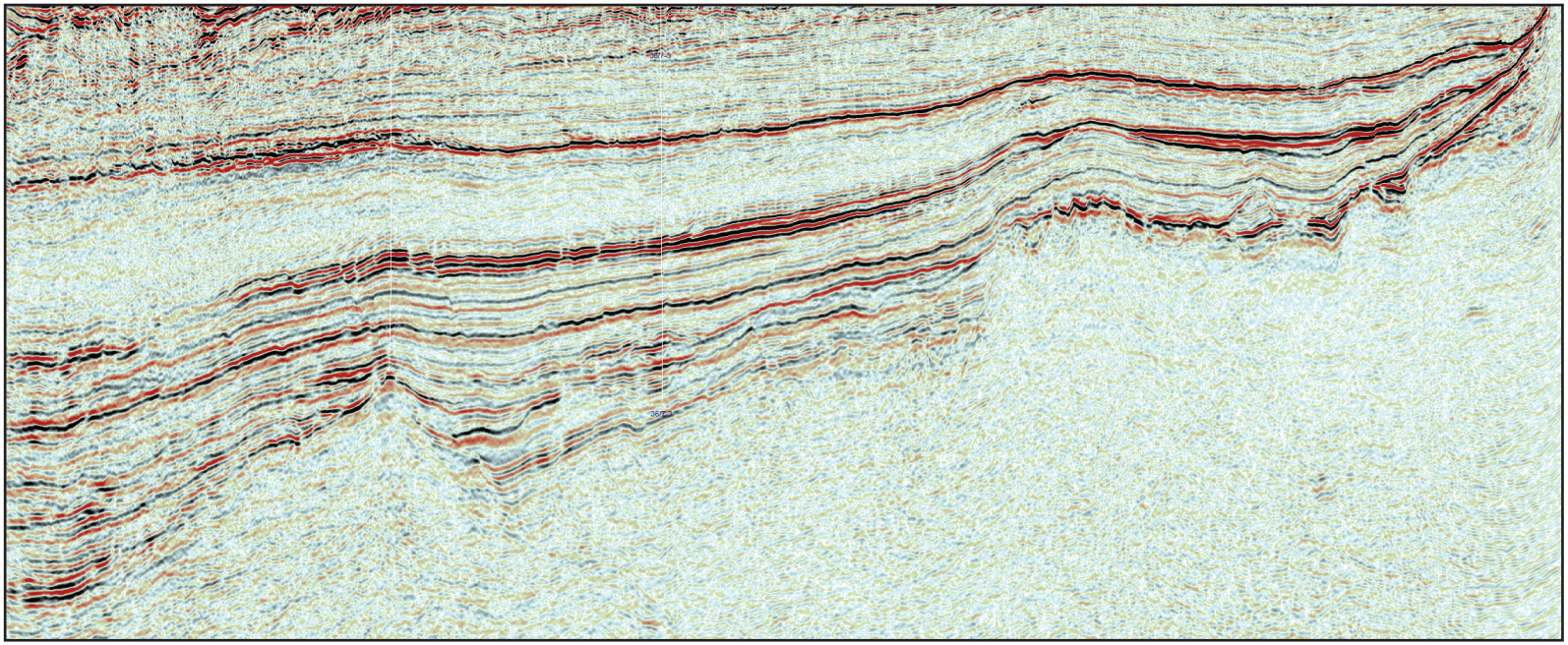

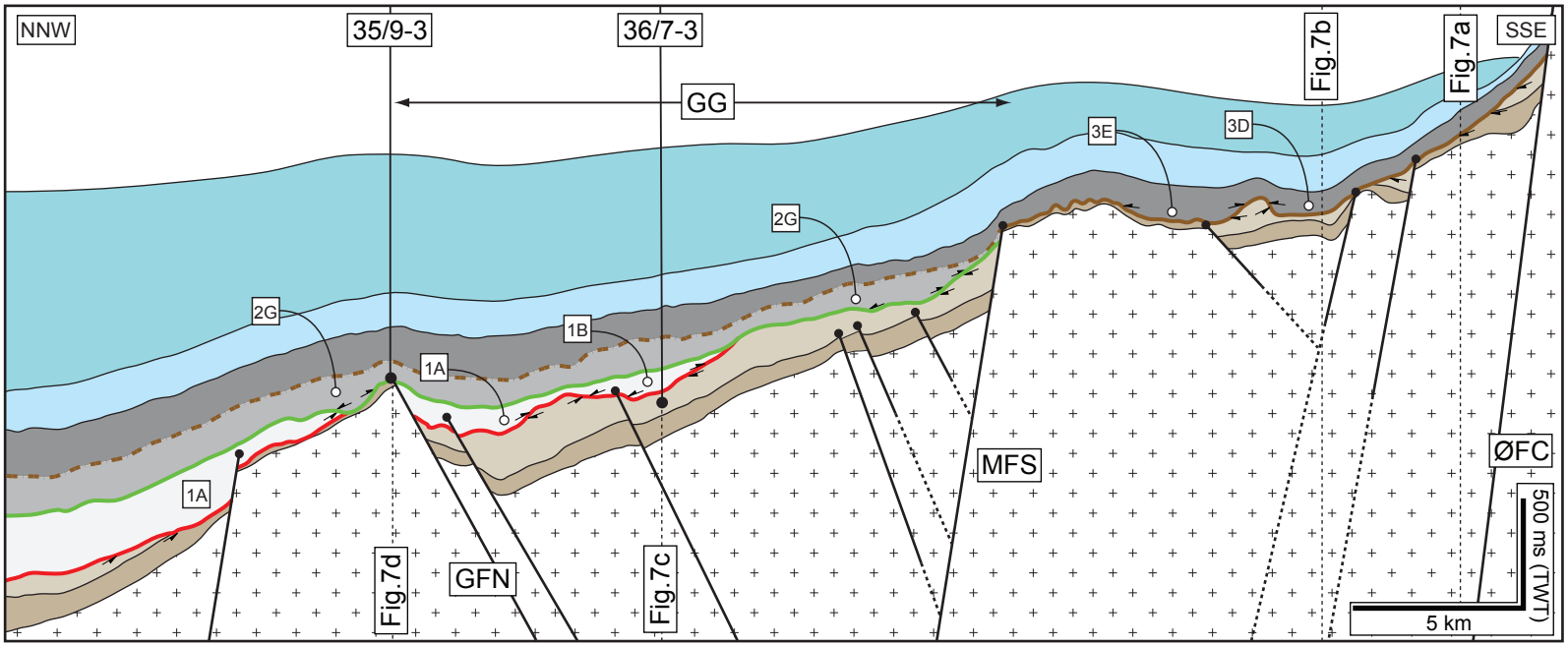
NNW
35/9-3
36/7-3
GG
Fig.7b
Fig.7a
SSE
3E
3D
2G
2G
1B
1A
1A
MFS
ØFC
Fig.7d
GFN
Fig.7c
600 ms (TWT)
5 km

Fig. 5

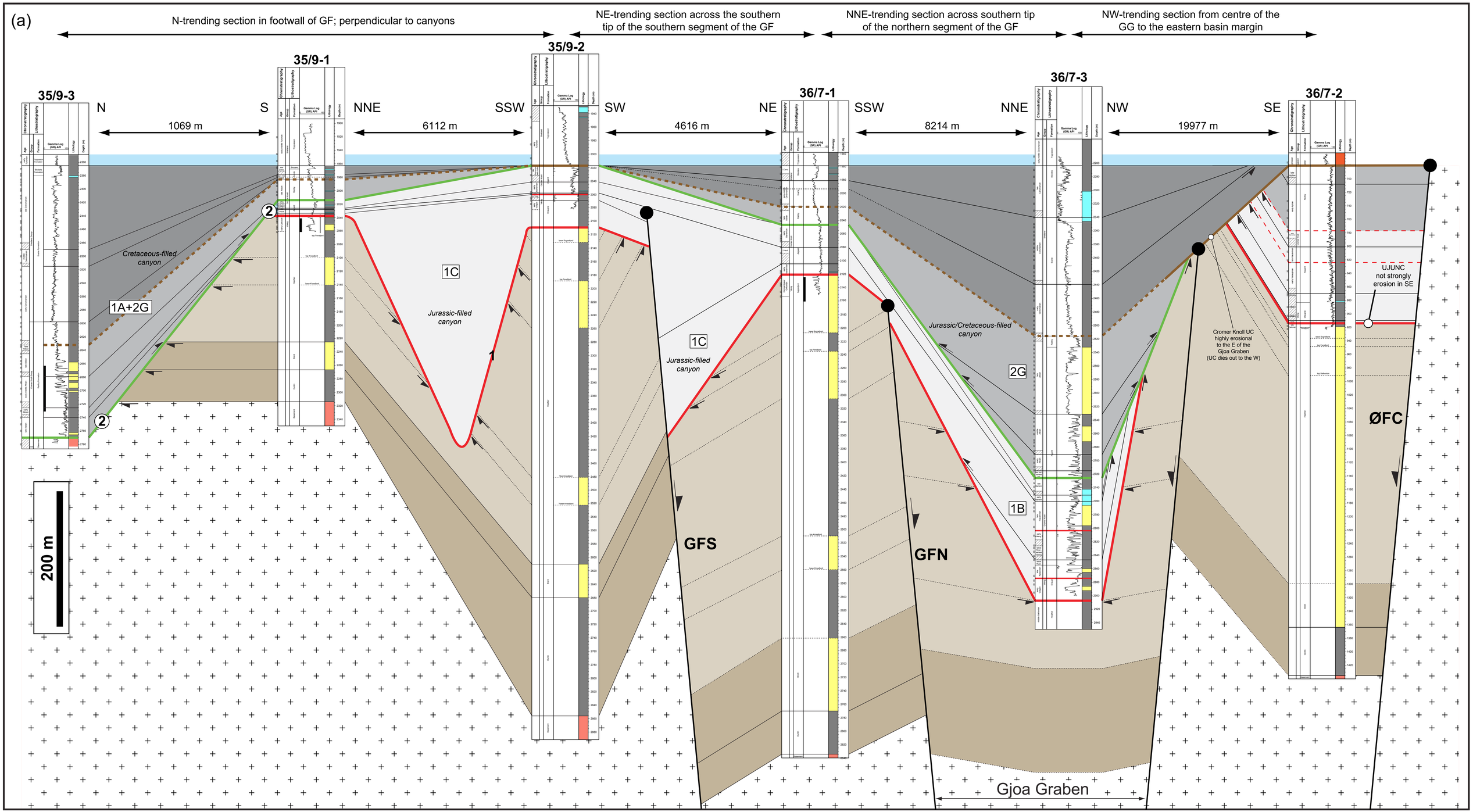
(a)
N-trending section in footwall of GF; perpendicular to canyons
NE-trending section across the southern tip of the southern segment of the GF
NNE-trending section across southern tip of the northern segment of the GF
NW-trending section from centre of the GG to the eastern basin margin
35/9-3
35/9-1
35/9-2
36/7-1
36/7-3
36/7-2
N
S
NNE
SSW
SW
NE
SSW
NNE
NW
SE
1069 m
6112 m
4616 m
8214 m
19977 m
Cretaceous-filled canyon
1A+2G
Jurassic-filled canyon
1C
Jurassic-filled canyon
1C
Jurassic/Cretaceous-filled canyon
2G
1B
Cromer Knoll UC highly erosional to the E of the Gjoa Graben (UC dies out to the W)
UJUNC not strongly erosion in SE
GFS
GFN
ØFC
Gjoa Graben
200 m

Fig. 5

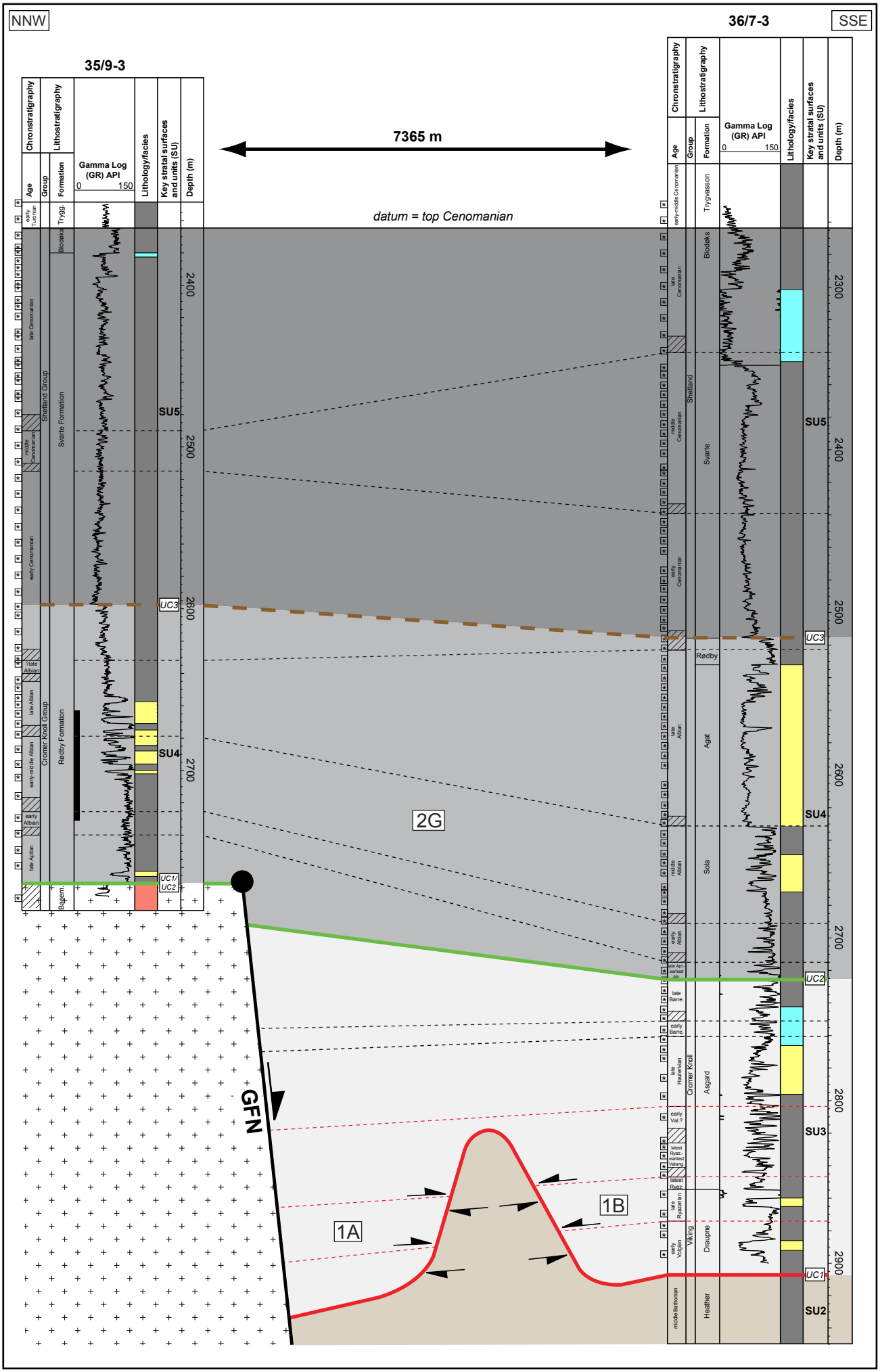
(b)
NNW
SSE
35/9-3
36/7-3
7365 m
datum = top Cenomanian
Chronstratigraphy
Lithostratigraphy
Age
Group
Formation
Gamma Log (GR) API
0
150
Lithology/facies
Key stratal surfaces and units (SU)
Depth (m)
Shetland Group
Svarte Formation
Rødby Formation
Cromer Knoll Group
Trygg.
Blodøks
Bagem.
Shetland
Svarte
Rødby
Agat
Sola
Cromer Knoll
Asgard
Viking
Draupne
Heather
Trygvasson
SU5
SU4
SU3
SU2
UC3
UC2
UC1
UC1/ UC2
2G
1A
1B
GFN
2400
2500
2600
2700
2800
2900

Fig. 5

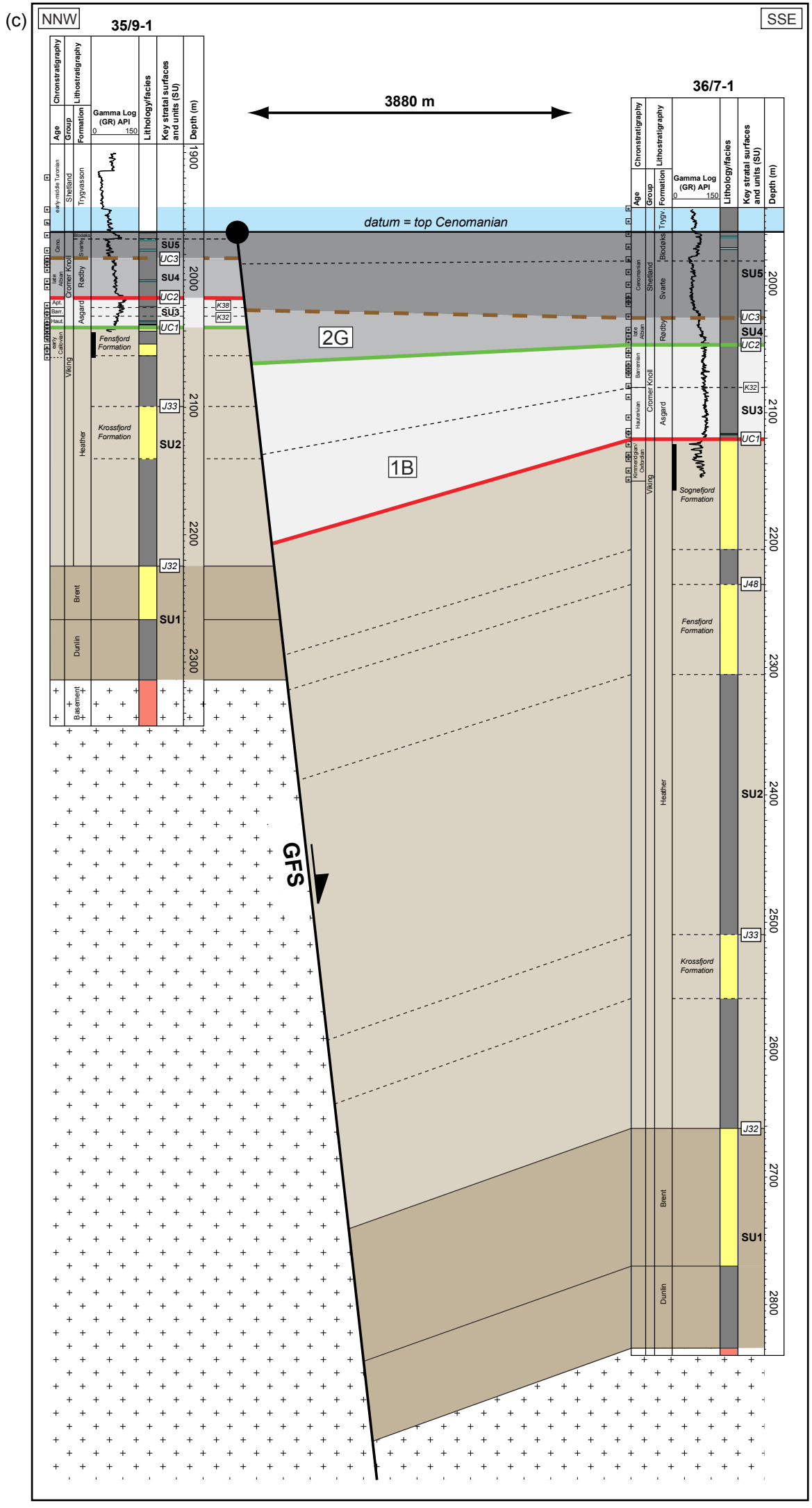
(c)
NNW
SSE
35/9-1
36/7-1
3880 m
datum = top Cenomanian
Chronstratigraphy
Lithostratigraphy
Age
Group
Formation
Gamma Log (GR) API
0
150
Lithology/facies
Key stratal surfaces and units (SU)
Depth (m)
SU5
UC3
SU4
UC2
SU3
UC1
SU2
SU1
J33
J32
K38
K32
J48
2G
1B
GFS
Fensfjord Formation
Krossfjord Formation
Sognefjord Formation
Cromer Knoll
Rødby
Asgard
Viking
Heather
Brent
Dunlin
Basement
Shetland
Trygvasson
Svarte
Blodøks
1900
2000
2100
2200
2300
2400
2500
2600
2700
2800

Fig. 6

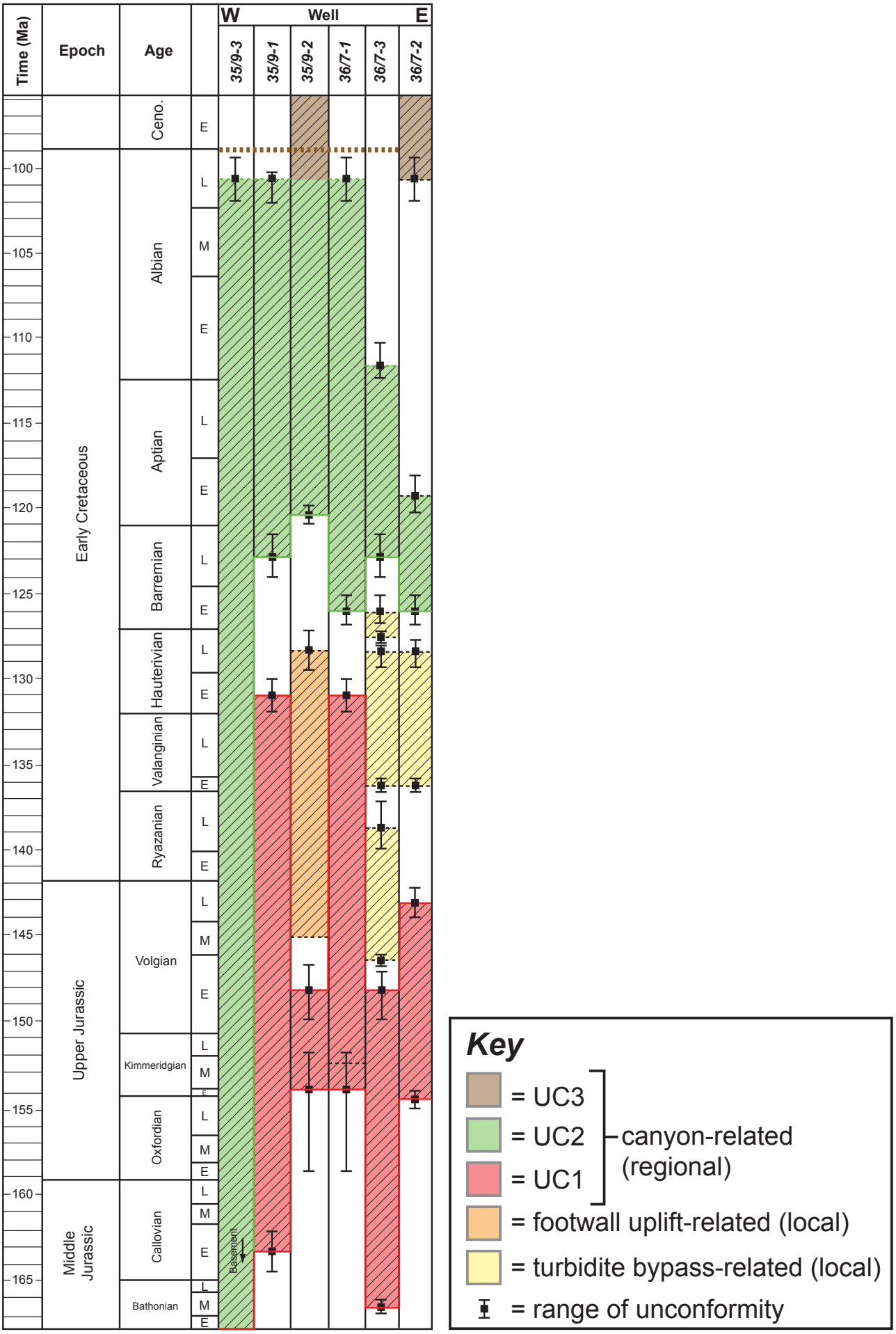
Time (Ma)
Epoch
Age
W
Well
E
35/9-3
35/9-1
35/9-2
36/7-1
36/7-3
36/7-2
Ceno.
Albian
Aptian
Barremian
Hauterivian
Valanginian
Ryazanian
Volgian
Kimmeridgian
Oxfordian
Callovian
Bathonian
Early Cretaceous
Upper Jurassic
Middle Jurassic
Basement
100
105
110
115
120
125
130
135
140
145
150
155
160
165
Key
= UC3
= UC2
= UC1
canyon-related (regional)
= footwall uplift-related (local)
= turbidite bypass-related (local)
= range of unconformity

Fig. 7

(a)

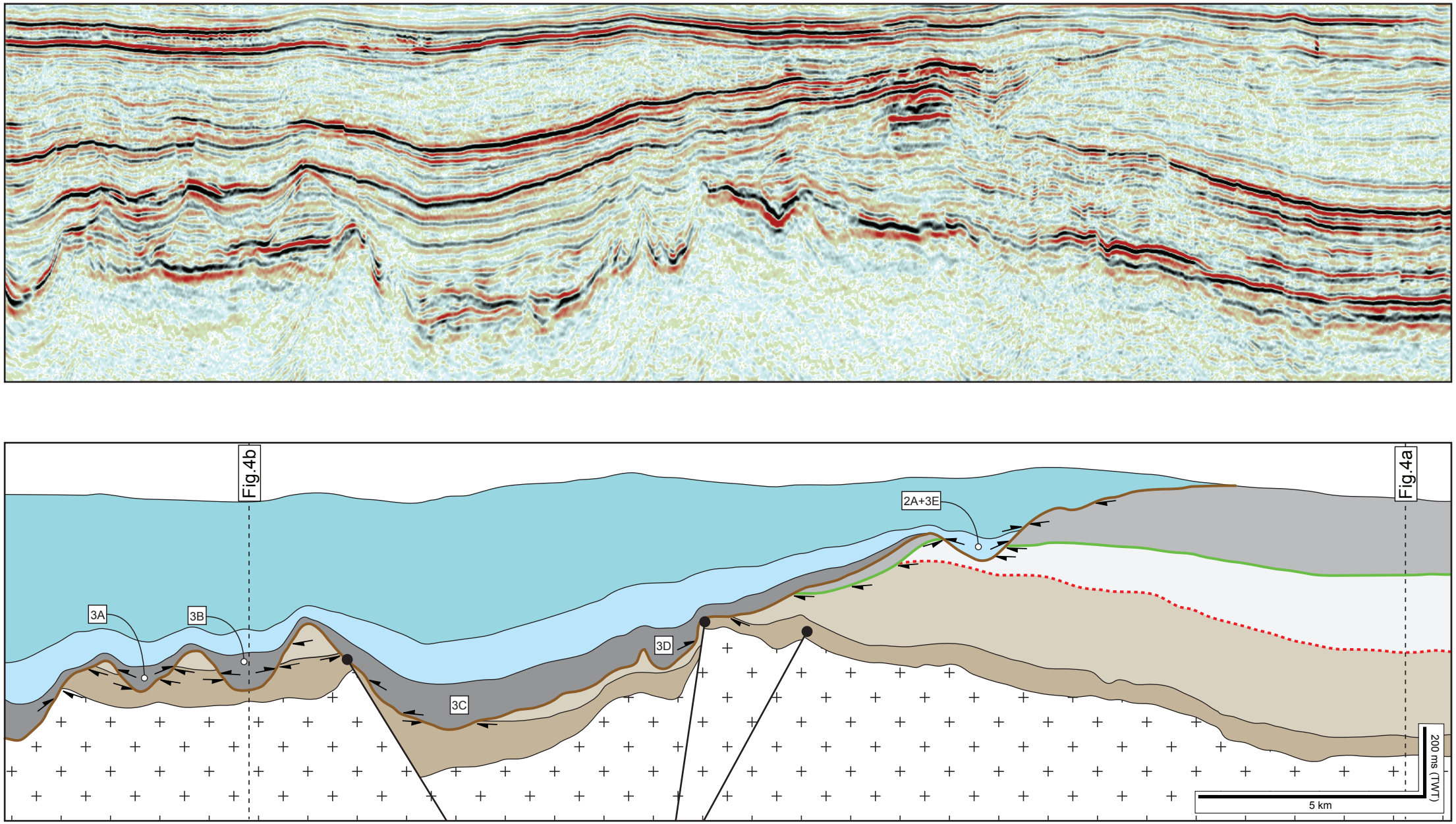

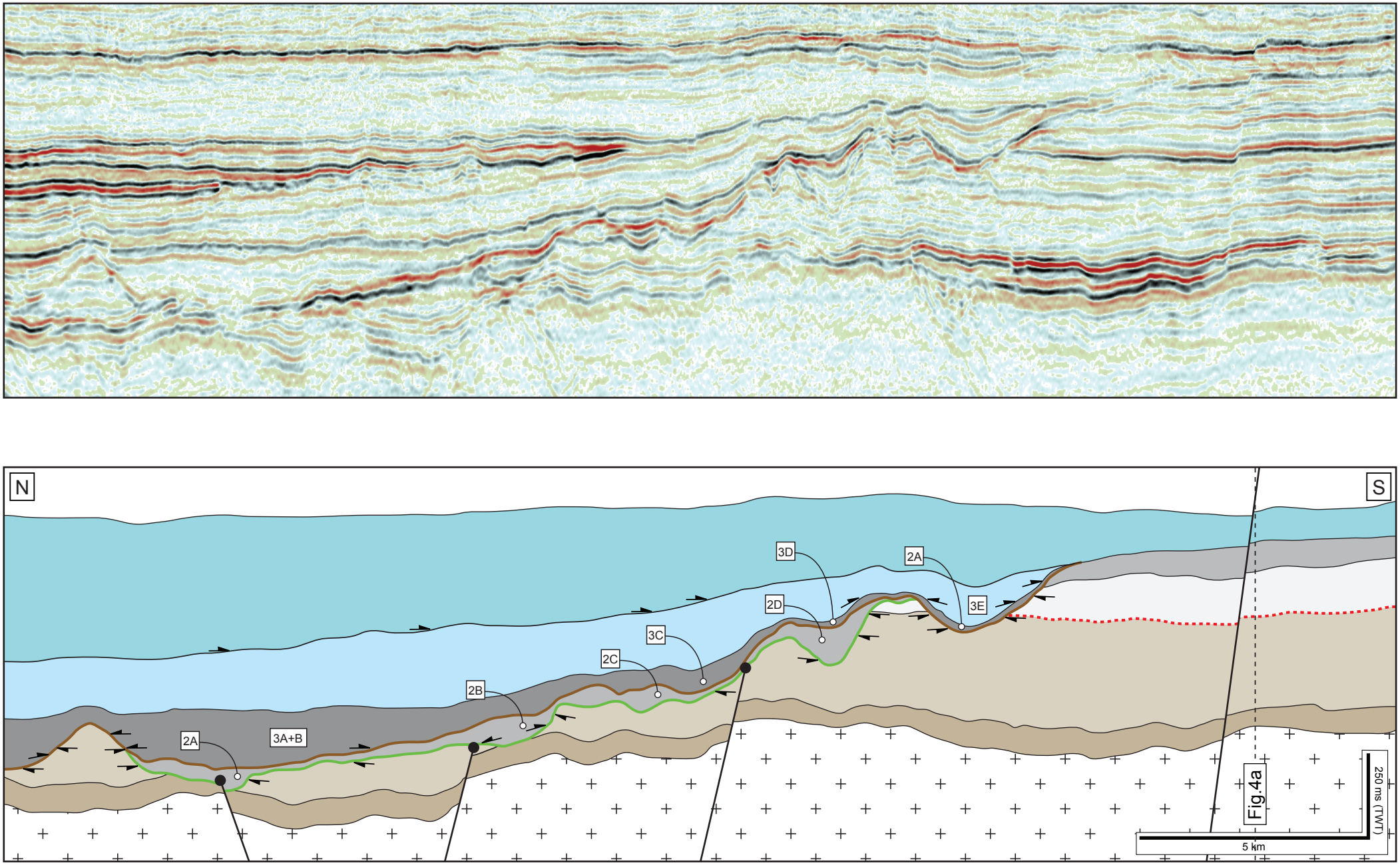
N
S
3D
2A
2D
3E
3C
2C
2B
2A
3A+B
Fig.4a
250 ms (TWT)
5 km

Fig. 7

(c)

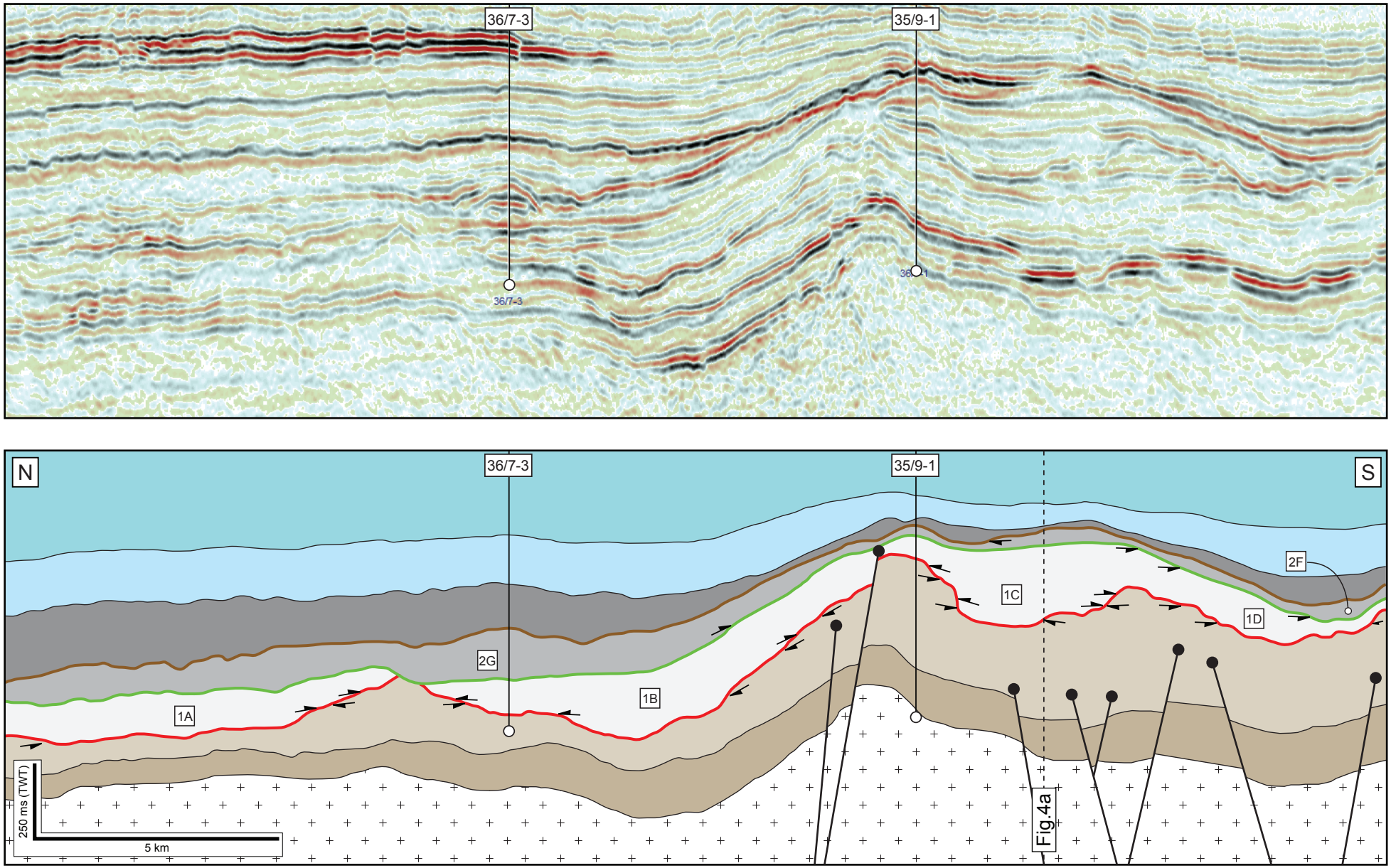

Fig. 7

(d)

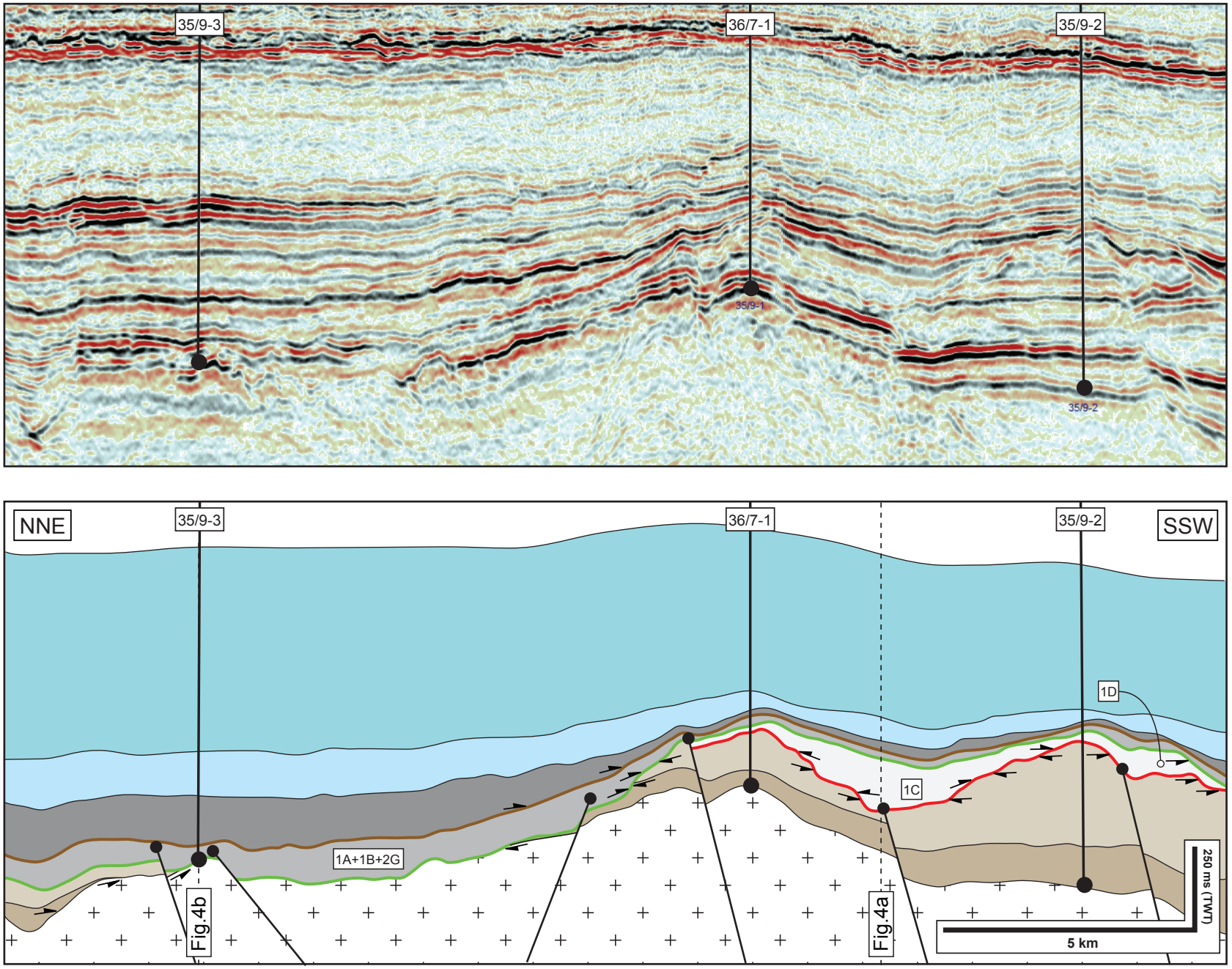
35/9-3
36/7-1
35/9-2
35/9-1
35/9-2
NNE
SSW
1D
1C
1A+1B+2G
Fig.4b
Fig.4a
250 ms (TWT)
5 km

Fig. 7

(e)

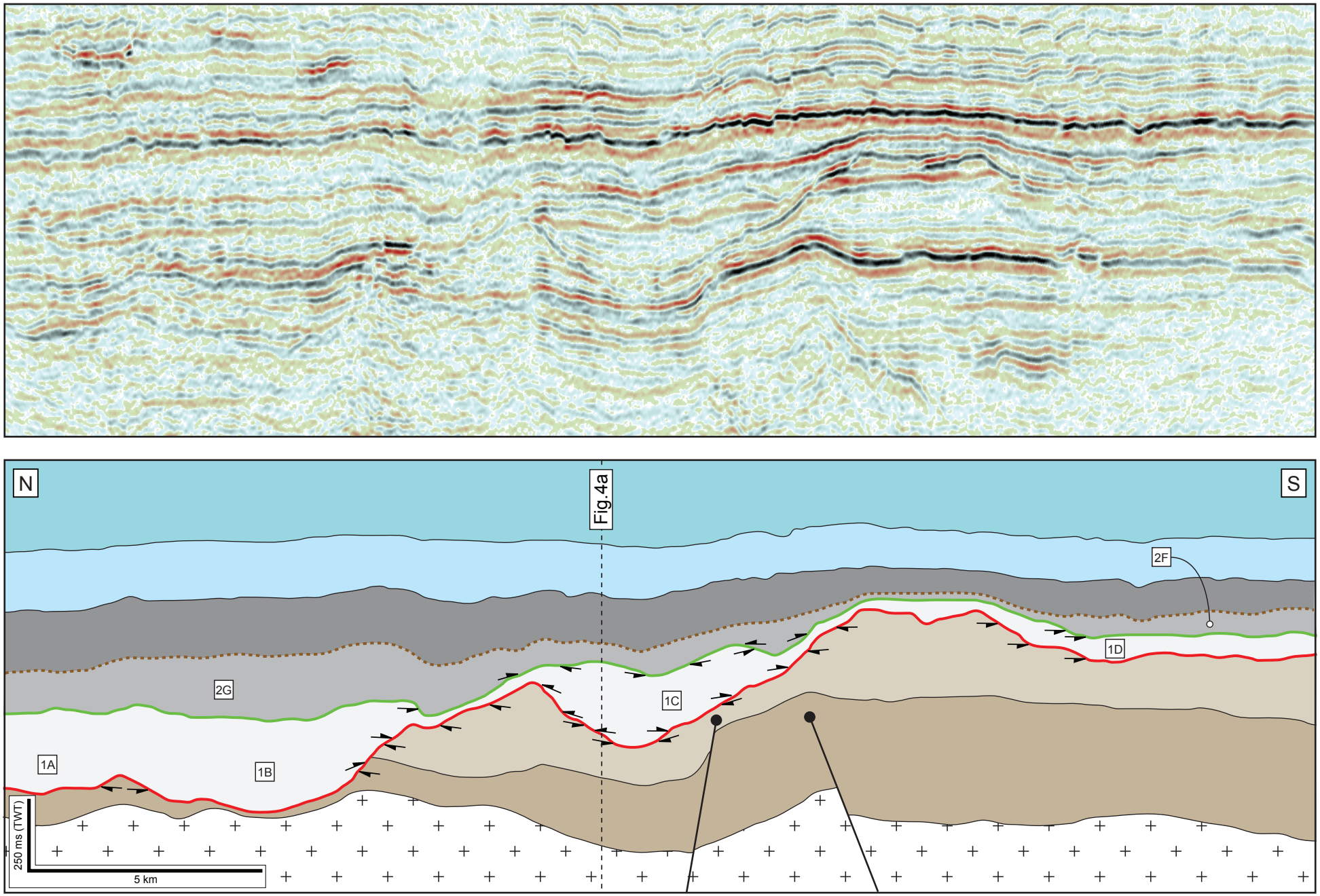

Fig. 8

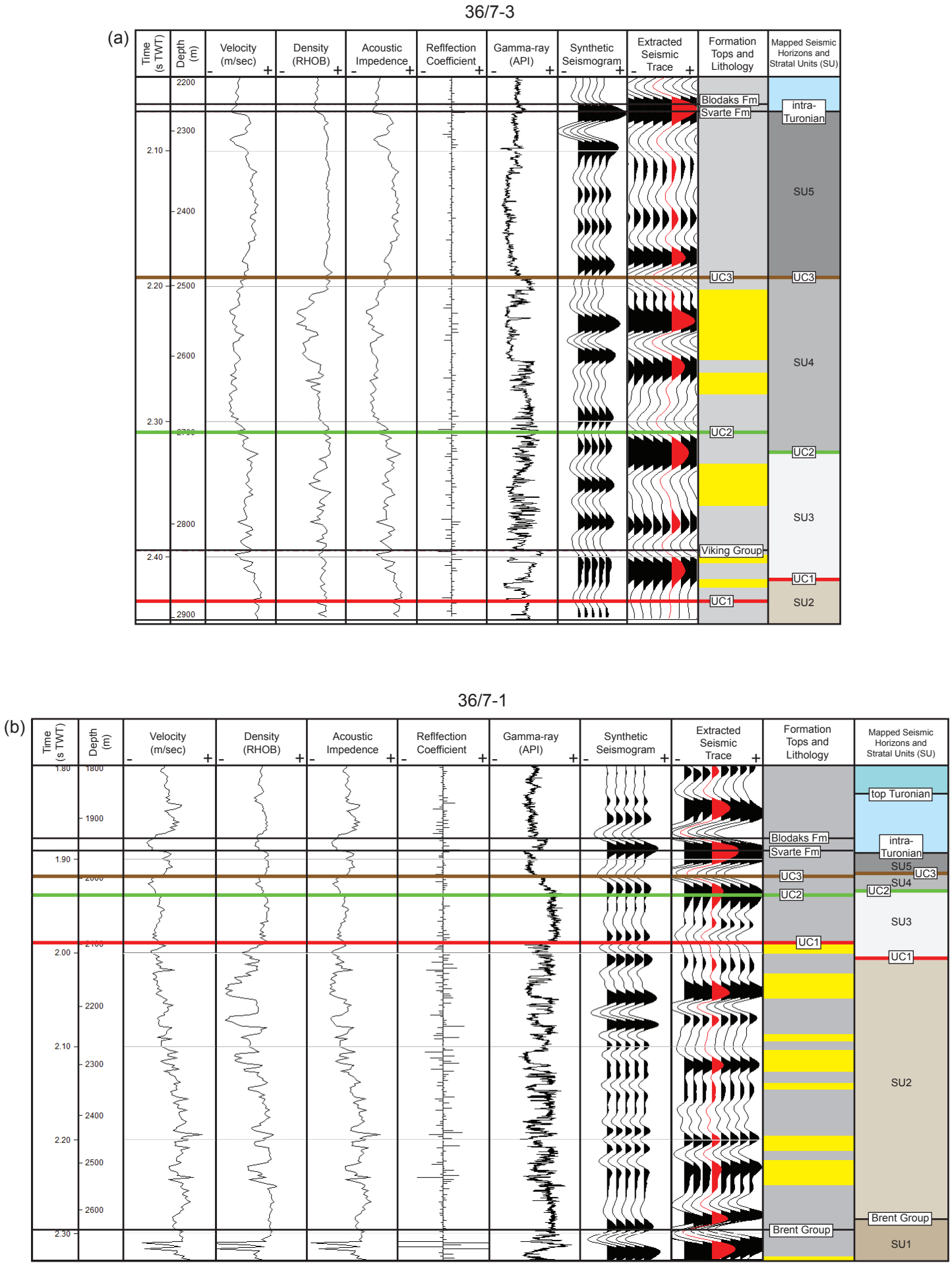
(a)
36/7-3
Time (s TWT)
Depth (m)
Velocity (m/sec)
Density (RHOB)
Acoustic Impedence
Reflfection Coefficient
Gamma-ray (API)
Synthetic Seismogram
Extracted Seismic Trace
Formation Tops and Lithology
Mapped Seismic Horizons and Stratal Units (SU)
Blodaks Fm
Svarte Fm
intra-Turonian
SU5
UC3
SU4
UC2
SU3
Viking Group
UC1
SU2
(b)
36/7-1
top Turonian
Brent Group
SU1

Fig. 9

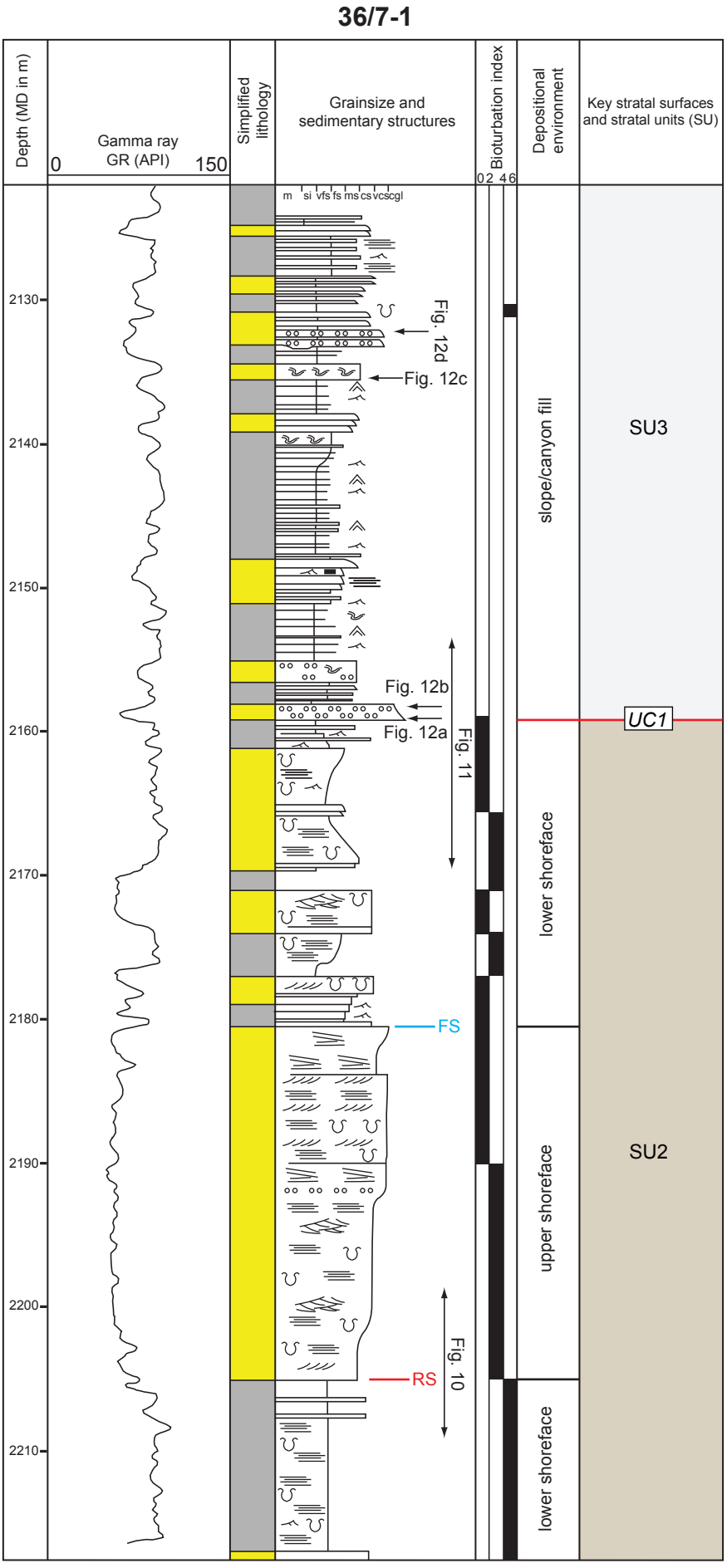
36/7-1
Depth (MD in m)
Gamma ray
GR (API)
0
150
Simplified lithology
Grainsize and sedimentary structures
m si vfs fs ms cs vcs cgl
Bioturbation index
0 2 4 6
Depositional environment
Key stratal surfaces and stratal units (SU)
2130
2140
2150
2160
2170
2180
2190
2200
2210
Fig. 12d
Fig. 12c
Fig. 12b
Fig. 12a
Fig. 11
Fig. 10
FS
RS
slope/canyon fill
lower shoreface
upper shoreface
lower shoreface
SU3
UC1
SU2

Fig. 10


NORSK HYDRO WELL: 36/7-1 CORE NO. 4
1 OF 28 TOP 2199.00 BTM 2200.00
2 OF 28 TOP 2200.00 BTM 2201.00
3 OF 28 TOP 2201.00 BTM 2202.00
4 OF 28 TOP 2202.00 BTM 2203.00
5 OF 28 TOP 2203.00 BTM 2204.00
NORSK HYDRO WELL: 36/7-1 CORE NO. 4
6 OF 28 TOP 2204.00 BTM 2205.00
7 OF 28 TOP 2205.00 BTM 2206.00
8 OF 28 TOP 2206.00 BTM 2207.00
9 OF 28 TOP 2207.00 BTM 2208.00
10 OF 28 TOP 2208.00 BTM 2209.00
RS

Fig. 11

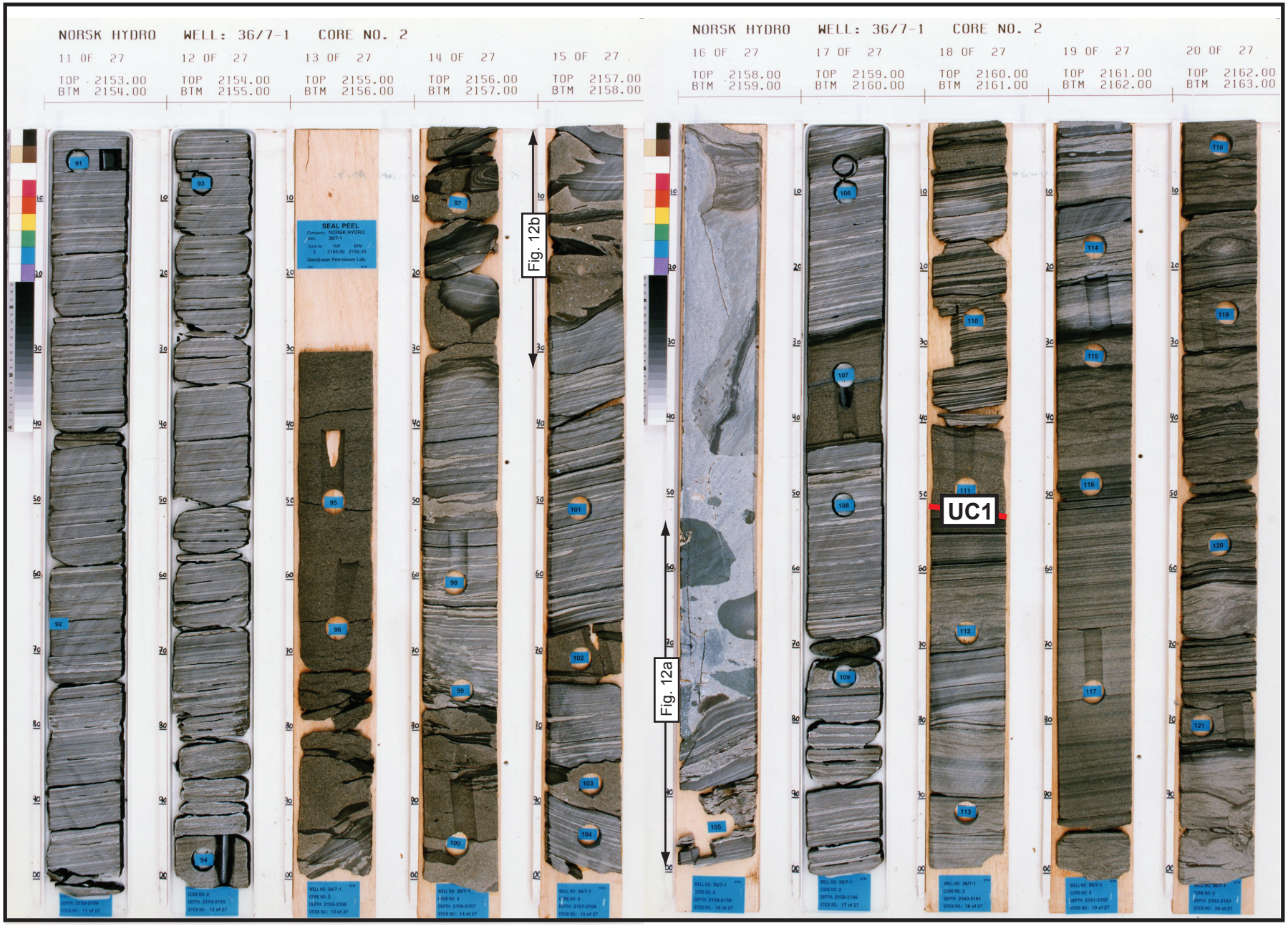
NORSK HYDRO WELL: 36/7-1 CORE NO. 2
11 OF 27 TOP 2153.00 BTM 2154.00
12 OF 27 TOP 2154.00 BTM 2155.00
13 OF 27 TOP 2155.00 BTM 2156.00
14 OF 27 TOP 2156.00 BTM 2157.00
15 OF 27 TOP 2157.00 BTM 2158.00
16 OF 27 TOP 2158.00 BTM 2159.00
17 OF 27 TOP 2159.00 BTM 2160.00
18 OF 27 TOP 2160.00 BTM 2161.00
19 OF 27 TOP 2161.00 BTM 2162.00
20 OF 27 TOP 2162.00 BTM 2163.00
SEAL PEEL
Fig. 12b
Fig. 12a
UC1

Fig. 12

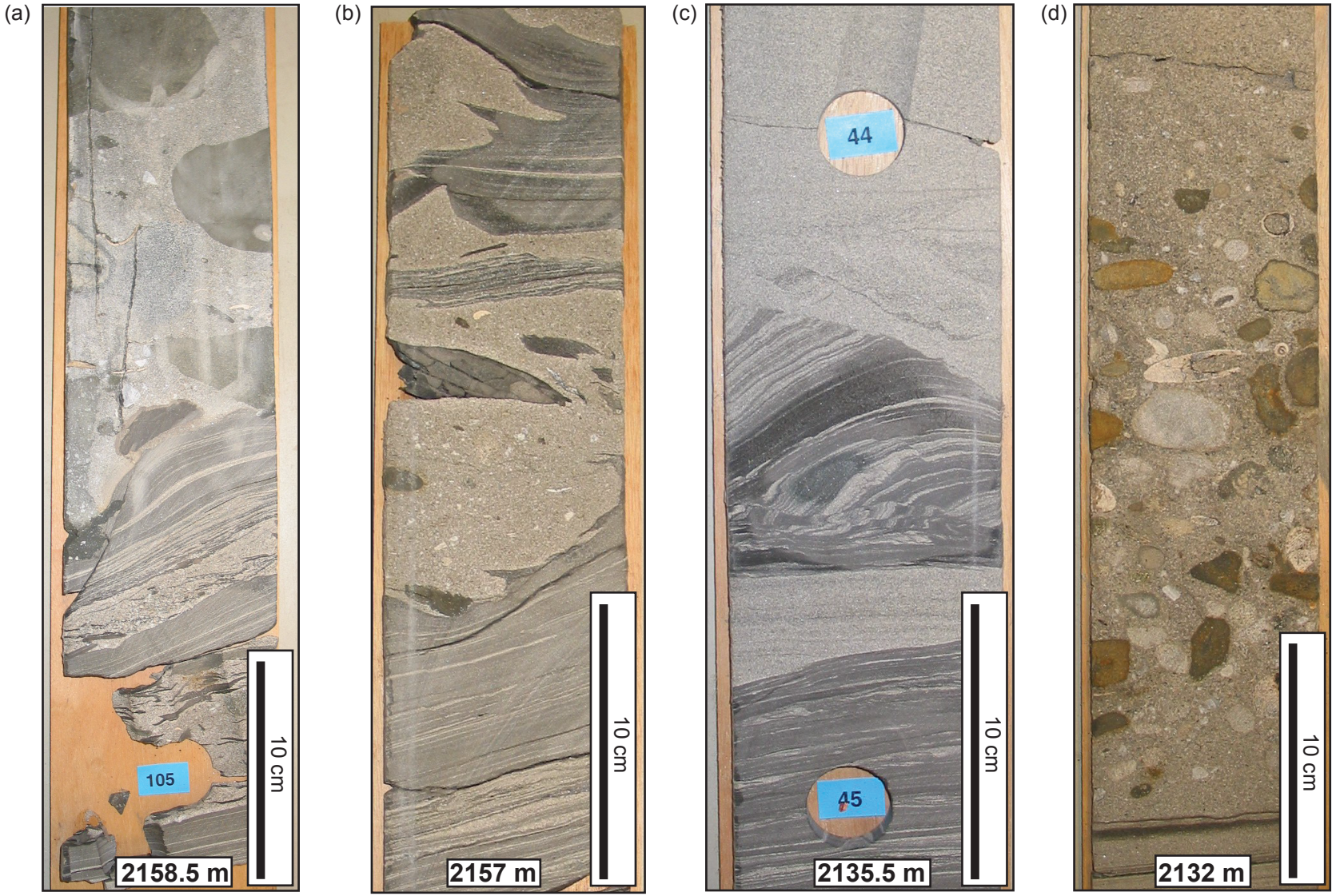

Fig. 13

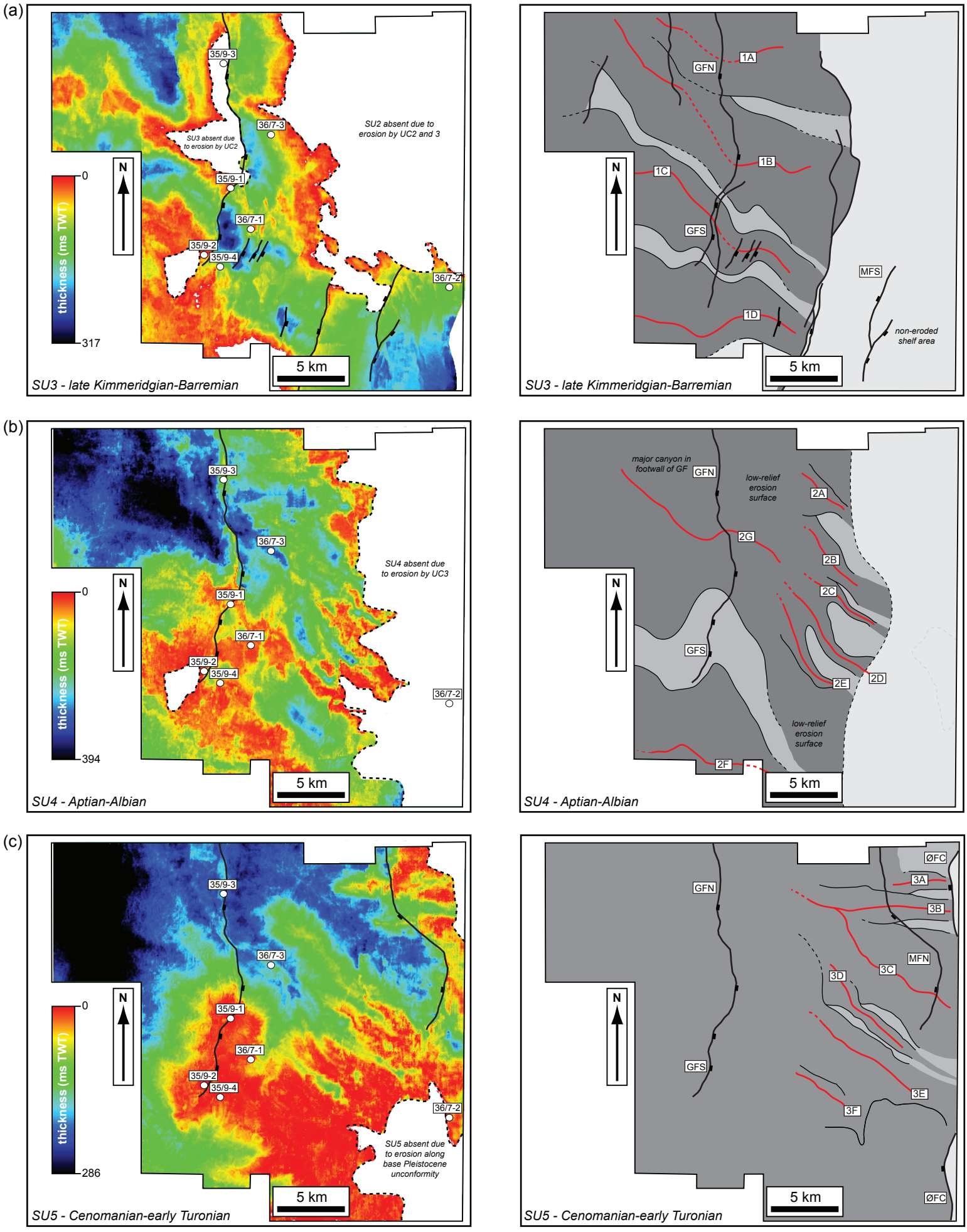
(a)
35/9-3
36/7-3
35/9-1
36/7-1
35/9-2
35/9-4
36/7-2
SU3 absent due to erosion by UC2
SU2 absent due to erosion by UC2 and 3
N
0
thickness (ms TWT)
317
5 km
SU3 - late Kimmeridgian-Barremian
GFN
1A
1B
1C
GFS
MFS
1D
non-eroded shelf area
5 km
SU3 - late Kimmeridgian-Barremian
(b)
35/9-3
36/7-3
35/9-1
36/7-1
35/9-2
35/9-4
36/7-2
SU4 absent due to erosion by UC3
N
0
thickness (ms TWT)
394
5 km
SU4 - Aptian-Albian
major canyon in footwall of GF
GFN
low-relief erosion surface
2A
2G
2B
2C
GFS
2E
2D
low-relief erosion surface
2F
5 km
SU4 - Aptian-Albian
(c)
35/9-3
36/7-3
35/9-1
36/7-1
35/9-2
35/9-4
36/7-2
SU5 absent due to erosion along base Pleistocene unconformity
N
0
thickness (ms TWT)
286
5 km
SU5 - Cenomanian-early Turonian
GFN
ØFC
3A
3B
MFN
3C
3D
GFS
3E
3F
ØFC
5 km
SU5 - Cenomanian-early Turonian

Table 1

	Well	Strata below unconformity	Strata above unconformity	Approximate stratigraphic gap (Myr)	Sedimentological expression	Comment
UC1	36/7-2	late Oxfordian-early Kimmeridgian	late Volgian	11	Deep marine mudstone on shallow marine sandstone	No seismic-scale erosional relief observed at well location
	35/9-2	early Kimmerdigian	early Volgian	6	Deep marine mudstone on shallow marine sandstone	Poor constraints on the age of strata (Sognefjord Fm) underlying the unconformity
	36/7-1	late Oxfordian-early Kimmeridgian	early Hauterivian	21.5	Deep marine mudstone on shallow marine sandstone	Poor constraints on the age of strata (Sognefjord Fm) underlying the unconformity
	35/9-3	Basement	late Aptian	>300	Deep marine mudstone and turbidite sandstone on gneiss	Forms part of a composite erosional unconformity with UC2 at the base of a major canyon
	35/9-1	early Callovian	early Hauterivian	32.5	Marls on shallow marine sandstone	
	36/7-3	middle Bathonian	early Volgian	18.5	Deep marine mudstone on shallow marine sandstone	
UC2	36/7-2	early Barremian	early Aptian	6.5	Deep marine mudstone on deep marine mudstone	No seismic-scale erosional relief observed at well location
	35/9-2	late Barremian-early Aptian	early Turonian	17	Marls on marine mudstones	Forms part of a composite erosional unconformity with UC3 on rift-related structural high
	36/7-1	early Barremian	late Albian	25.5	Deep marine mudstone on deep marine mudstone	
	35/9-3	Basement	late Aptian	>300	Deep marine mudstone and turbidite sandstone on gneiss	Forms part of a composite erosional unconformity with UC1 at the base of a major canyon
	35/9-1	late Barremian	late Albian	22.5	Marls on deep marine mudstones	
	36/7-3	late Barremian	late Aptian-earliest Albian	11.5	Deep marine mudstone on deep marine mudstone	
UC3	36/7-2	late Aptian	Ypresian	155.5	Volcanic tuffs on deep marine mudstone	Forms part of a composite erosional unconformity related to post-Cretaceous uplift of western Norway
	35/9-2	late Barremian-early Aptian	early Turonian	20	Marls on deep marine mudstones	Composite (erosional) unconformity with UC2 on rift-related structural high
	36/7-1	late Albian	early Cenomanian-middle Cenomanian	0	Marls on deep marine mudstones	No biostratigraphically-defined unconformity (although questionable presence of early Cenomanian)
	35/9-3	early Cenomanian	early Cenomanian	0	Deep marine mudstone on deep marine mudstone	No biostratigraphically-defined unconformity
	35/9-1	late Albian	early Cenomanian-middle Cenomanian	0	Marls on deep marine mudstones	No biostratigraphically-defined unconformity (although questionable presence of early Cenomanian)
	36/7-3	late Albian	early Cenomanian	0	Marls on deep marine mudstone	No biostratigraphically-defined unconformity